



Iodine oxoacids and their roles in sub-3 nm particle growth in polluted urban environments

Ying Zhang^{1,2,3,★}, Duzitian Li^{2,3,★}, Xu-Cheng He^{4,5}, Wei Nie^{2,3}, Chenjuan Deng⁶, Runlong Cai⁴, Yuliang Liu^{2,3}, Yishuo Guo¹, Chong Liu^{2,3}, Yiran Li⁶, Liangduo Chen^{2,3}, Yuanyuan Li^{2,3}, Chenjie Hua¹, Tingyu Liu¹, Zongcheng Wang¹, Jiali Xie¹, Lei Wang^{2,3}, Tuukka Petäjä⁴, Federico Bianchi⁴, Ximeng Qi^{2,3}, Xuguang Chi^{2,3}, Pauli Paasonen⁴, Yongchun Liu¹, Chao Yan^{2,3}, Jingkun Jiang⁶, Aijun Ding^{2,3}, and Markku Kulmala^{1,2,3,4}

¹Aerosol and Haze Laboratory, Beijing Advanced Innovation Center for Soft Matter Science and Engineering, Beijing University of Chemical Technology, Beijing, China

²Joint International Research Laboratory of Atmospheric and Earth System Sciences, School of Atmospheric Sciences, Nanjing University, Nanjing, China

³Jiangsu Provincial Collaborative Innovation Center of Climate Change, Nanjing, China

⁴Institute for Atmospheric and Earth System/Physics, Faculty of Science, University of Helsinki, Helsinki, Finland

⁵Yusuf Hamied Department of Chemistry, University of Cambridge, Cambridge, CB2 1EW, UK

⁶State Key Joint Laboratory of Environment Simulation and Pollution Control, State Environmental Protection Key Laboratory of Sources and Control of Air Pollution Complex, School of Environment, Tsinghua University, Beijing, China

★These authors contributed equally to this work.

Correspondence: Xu-Cheng He (xucheng.he@helsinki.fi) and Wei Nie (niewei@nju.edu.cn)

Received: 21 February 2023 – Discussion started: 21 March 2023

Revised: 12 December 2023 – Accepted: 22 December 2023 – Published: 12 February 2024

Abstract. New particle formation contributes significantly to the number concentration of ultrafine particles (UFPs, $d \leq 100$ nm) and has a great impact on human health and global climate. Iodine oxoacids (HIO_x , including iodic acid, HIO_3 , and iodous acid, HIO_2) have been observed in pristine regions and proved to dominate new particle formation (NPF) at some sites. However, the knowledge of HIO_x in polluted urban areas is rather limited. Here, we conducted a long-term measurements of gaseous iodine oxoacids and sulfuric acid in Beijing from January 2019 to October 2021 and also in Nanjing from March 2019 to February 2020 and investigated the contribution of HIO_x to UFP number concentration in both urban environments. HIO_3 is highest in summer, up to 2.85×10^6 and $2.78 \times 10^6 \text{ cm}^{-3}$ in Beijing and Nanjing, respectively, and is lowest in winter by 96 % and 75 %, respectively. HIO_3 exhibits more prominent variation than H_2SO_4 in both urban sites. HIO_3 concentration shows a clear diurnal pattern at both sites with a daily maximum at around noontime, similar to the atmospheric temperature, solar radiation, and ozone (O_3) levels. HIO_2 concentration has the same diurnal and seasonal trend as HIO_3 but is overall about an order of magnitude lower than HIO_3 concentration. Back trajectory analysis suggests that the sources for inland iodine species could be a mix of marine and terrestrial origins, with both having peak iodine emission in warm seasons. While the contribution of HIO_2 to particle growth is marginal in Beijing and Nanjing, our results demonstrate that HIO_3 enhances the particle survival probability of sub-3 nm particles by about 40 % (median) and occasionally by more than 100 % in NPF events, suggesting HIO_x are significant contributor to UFPs in polluted urban areas. As the growth contribution from HIO_3 and H_2SO_4 is similar on a per-molecule basis, we propose that the sum of HIO_3 and H_2SO_4 could be used to estimate sub-3 nm particle growth of inorganic acid origin in polluted atmospheres with a significant amount of HIO_x .

1 Introduction

Aerosol particles are ubiquitous in Earth's atmosphere and have both primary and secondary sources (Kulmala et al., 2004b). Primary aerosol emissions stem from natural sources, including sea spray, soil mineral dust, biomass burning, and volcanic debris (Tomasi and Lupi, 2017), and anthropogenic sources such as fuel combustion, industrial processes, and transportation (Tomasi and Lupi, 2017). Besides direct emissions, atmospheric new particle formation (NPF), a secondary particle source, plays a significant role in increasing aerosol population (Kulmala et al., 2012). Only a few vapors, such as sulfuric acid (H₂SO₄), water vapor (H₂O), ammonia (NH₃), amines (e.g., dimethylamine, C₂H₇N), and highly oxygenated organic molecules (HOMs), are widely confirmed to nucleate and form new particles under appropriate atmospheric conditions (Kulmala et al., 2004a; Kürten et al., 2016; Li et al., 2020; Almeida et al., 2013; Kirkby et al., 2011, 2016; Lehtipalo et al., 2018; Tröstl et al., 2016; Yao et al., 2018). Once growing past the critical sizes (e.g., 50 to 100 nm), these newly formed particles can be activated as cloud condensation nuclei (CCN), which in turn influence cloud formation and have climatic effects (Kerminen et al., 2005; Kalkavouras et al., 2019; Jiang et al., 2021). Additionally, NPF is a dominant source of atmospheric ultrafine particles in polluted urban environments (Yan et al., 2021). These small particles (≤ 100 nm) can penetrate into the respiratory system, thus posing health risks to human beings (Chen et al., 2016; Downward et al., 2018). Therefore, understanding NPF is important both in terms of evaluating climate change and understanding the health risks of aerosols (Kulmala et al., 2022).

Due to its chemically complex nature, the understanding of the key precursor vapors and controlling mechanisms of urban NPF is still limited. Gaseous sulfuric acid and dimethylamine (DMA, C₂H₇N) are believed to play important roles in aerosol nucleation in urban environments (Xiao et al., 2021; R. Cai et al., 2021c, 2022b; Almeida et al., 2013; Yao et al., 2018). A recent study quantitatively demonstrated the decisive role of H₂SO₄ in initiating nucleation with the presence of stabilizers such as amines and NH₃ in Beijing (Yan et al., 2021). The subsequent growth of fresh particles is contributed to by both H₂SO₄ and oxidized organic vapors depending on the particle sizes. In Beijing, it was suggested that H₂SO₄ and its clusters contribute significantly to the growth of 1.5–3 nm particles (Deng et al., 2020b) while gas-phase oxygenated organic molecules (OOMs) promote the growth of 3–25 nm particles (Qiao et al., 2021).

Besides these widely studied species, oxidized iodine compounds were also found to introduce rapid particle formation, mostly observed in mid-latitude coastal sites (Hoffmann et al., 2001; Mäkelä, 2002; O'Dowd et al., 2002). Iodine nucleation was conventionally thought to be initi-

ated by iodine oxides (Jimenez, 2003; Gomez Martin et al., 2020; O'Dowd and Hoffmann, 2005; Hoffmann et al., 2001; O'Dowd et al., 2002). However, field observations at the Mace Head observatory and dedicated experiments carried out in the CLOUD chamber at CERN revealed iodine oxoacids (HIO_x, i.e., HIO₃, and HIO₂ in this study) as the key nucleating species in pristine regions (Zhang et al., 2022; He et al., 2021b). With state-of-the-art mass spectrometric methods, iodine oxoacids were recently identified in locations other than mid-latitude coastal sites, such as in Arctic sites (Baccarini et al., 2020; Beck et al., 2021; Sipilä et al., 2016; He et al., 2021b), Antarctic sites (Jokinen et al., 2018; He et al., 2021b), boreal forest sites (Jokinen et al., 2022; He et al., 2021b), a remote marine site (He et al., 2021b), and importantly also in polluted urban sites (He et al., 2021b). Chamber experiments have shown that HIO₃ (stabilized by HIO₂) nucleates faster than H₂SO₄ with 100 pptv NH₃ at the same temperature and equal acid concentrations, although iodine oxoacid nucleation rates are still lower than H₂SO₄-DMA nucleation (He et al., 2021b). It is worthwhile to note that the nucleation involving both iodine oxoacids and DMA remains unclear and that iodine oxoacid nucleation may be further enhanced by strong bases (e.g., different amines) in urban environments. After the formation of fresh particles, HIO₃ dominates the growth of iodine particles between 1.8 and 3.2 nm at growth rates equal to those of H₂SO₄ (He et al., 2021b). It can be expected that iodine oxoacids will contribute at least to sub-3 nm particle growth, and potentially also to particle nucleation, in polluted urban environments. Therefore, iodine oxoacids have the potential to enhance the survival probability (Lehtinen et al., 2007) of fresh particles in the urban environment.

In order to quantitatively understand the contribution of iodine oxoacids in urban particle formation, we conducted a long-term measurement of iodine oxoacids and sulfuric acid (H₂SO₄) in urban Beijing from January 2019 to October 2021, and in suburban Nanjing from March 2019 to February 2020. Diurnal and seasonal trends of iodine and sulfur oxoacids are analyzed, and the potential sources of the unexpected iodine oxoacids are discussed. Moreover, we quantitatively discuss the contribution of HIO₃ to aerosol growth rate below 3 nm (GR_{<3nm}) and the potential enhancement in particle survival probability. Our study provides the first long-term observations of iodine oxoacids in polluted urban environments which could contribute to aerosol formation studies in inland cities.

2 Methods

2.1 Measurement sites and instruments

2.1.1 Sites

Measurements in urban Beijing were conducted from January 2019 to October 2021 on the fifth floor of the teaching building at the west campus of Beijing University of Chemical Technology (Aerosol and Haze Laboratory (AHL)/BUCT station, 39°56' N, 116°17' E). Located about 150 km away from the nearest coastline in the southeast, the station is surrounded by residential buildings and three main roads, and a detailed description of this site can be found in a previous study (Liu et al., 2020). The observations in Nanjing were conducted at the Station for Observing Regional Process of Earth System (SORPES; 32°07' N, 118°57' E), a research and experiment platform inside Nanjing University, Xianlin Campus, 20 km northeast of downtown Nanjing and about 190 km away from the nearest coastline in the east. Because of its unique geophysical location, SORPES station is considered to be a regional background station under the influence of anthropogenic plume from the YRD (Yangtze River Delta) city cluster and multiscale transport coupled with Asian monsoon (Ding et al., 2016). The geophysical distribution of two sites can be found in Fig. S1 in the Supplement.

2.1.2 Acid concentrations

Gaseous iodine oxoacids (HIO₃ and HIO₂) and H₂SO₄ were detected by the nitrate-CIMS (Aerodyne Research Inc. and Tofwerk AG) composed of a chemical ionization (CI) source and an atmospheric pressure interface time-of-flight mass spectrometer (APi-TOF). Two long time-of-flight mass analyzers (LToF, resolution at around 10 000 Th Th⁻¹) were used at the AHL/BUCT station from January 2019 to October 2021 and at SORPES station from March 2019 to December 2019, respectively, while a lower resolution time-of-flight analyzer (HToF, resolution at around 5000 Th Th⁻¹) was utilized at the SORPES station from January 2020 to February 2020. As the comprehensive description of nitrate-CIMS has been given in previous works (Junninen et al., 2010; Jokinen et al., 2012), they are only briefly discussed here. Ambient air was drawn into a laminar flow reactor through a 0.75 in. (1.91 cm) diameter stainless steel tube with a sample flow of about 7.2 L min⁻¹ and surrounded by a purified airflow of 32 L min⁻¹ serving as the sheath flow at the AHL/BUCT station and 25 L min⁻¹ at the SORPES station. The dominant reagent ions were nitrate ions (NO₃⁻ and HNO₃NO₃⁻ and HNO₃HNO₃NO₃⁻), which were generated in the sheath flow by exposing gaseous nitric acid in the sheath flow to a photo ionizer X-ray (Model L9491, Hamamatsu, Japan). The data of nitrate-CIMS were acquired at 1 Hz time resolution and analyzed with the MATLAB (MathWorks Inc.) toolbox ToFTools package (version 6.11) (Junninen et al., 2010).

H₂SO₄ calibration was conducted using a standardized method (Kurten et al., 2012; He et al., 2023). In a nutshell, the calibration of H₂SO₄ involved the reaction of an excessive amount of sulfur dioxide (SO₂) with a known quantity of hydroxyl (OH) radicals generated by a portable mercury lamp. This mercury lamp is equipped with a filter to intercept the sample air containing water, which, in turn, is photolyzed to produce OH radicals. The convection–diffusion reaction processes within the chemical ionization inlet can be accurately simulated using a two-dimensional model (e.g., the MARFORCE-Flowtube model) (He et al., 2023), allowing for the quantification of H₂SO₄ concentration at the mass spectrometer's entrance. The quantification of the measured signals for H₂SO₄ monomer at both sites are seasonal calibrated with diffusion losses in tube into consideration. Since both H₂SO₄ and HIO_x are detected at the collision limit, they share the same calibration factor (He et al., 2021b, 2023). The general systematic error for the detection of H₂SO₄ and HIO_x is expected to be within 50 % to 200 % (Liu et al., 2021).

2.1.3 Particle number size distribution

The particle number size distribution (PNSD) from approximately 1 nm to 10 μm at the AHL/BUCT station was measured. This was done using a diethylene glycol scanning mobility particle spectrometer (DEG-SMPS, 1–4.5 nm) (Jiang et al., 2011), equipped with a miniature cylindrical differential mobility analyzer (mini-cy DMA) (Cai et al., 2017a). In addition, we utilized a homemade particle size distribution system (PSD, 3 nm–10 μm) (Liu et al., 2016). At the SORPES station, the PNSD was measured using an aerodynamic particle sizer (APS, TSI, APS-3321, USA, 500–1000 nm) and two SMPSs equipped with a TSI long-DMA (TSI Inc., model 3081) and a TSI nano-DMA (TSI Inc., model 3085). Additionally, ions of sizes ranging from 0.8 to 42 nm were measured using a neutral cluster and air ion spectrometer (NAIS, Airel Ltd., Estonia) (Manninen et al., 2016) in Nanjing.

2.1.4 O₃ concentration and other meteorological factors

The ozone (O₃) concentration was measured using ozone analyzers (49i, Thermo Fisher Scientific Inc. USA) at both sites. Additionally, ambient meteorological factors, including temperature (*T*), relative humidity (RH), and ultraviolet B radiation (UVB) were measured using an Automatic Weather Station (AWS310, Vaisala Inc.) in Beijing, whereas *T*, RH, and downward short-wave radiation (DSR) were recorded by sensors at the height of 44 m above the ground level at the SORPES station. The *T* and RH were measured by a temperature and relative humidity probe (HMP155A, Campbell Inc., USA), and the DSR was recorded by a CNR4 net radiometer (OTT Hydromet Corp. Germany).

2.2 Data analysis

2.2.1 Characteristic of NPF events from PNSD

According to a widely used method (Kulmala et al., 2012), we classified all of the measurement days into NPF and non-NPF events at both sites. All undefined days were regarded as non-NPF events in this study. Furthermore, NPF events exhibiting obvious nucleation and clear growth of fresh nucleation particles were categorized as “NPF-A”, while the remaining NPF events were designated as “NPF-B”. Since there were periods when some key instruments failed to work, the NPF frequencies in each month were calculated as the ratio of the NPF event days to the days with valid data. The monthly statistics at both sites were summarized in Table S1. From the measured particle number size distribution, we calculated the condensation sink (CS) (Laakso et al., 2004; Kulmala et al., 2012), coagulation sink (CoagS) (Kulmala et al., 2001), and growth rate (GR) for the NPF events.

CS, which characterizes the loss rate of gaseous precursors and clusters onto the particles (Lehtinen et al., 2003), was calculated using Eq. (1) (Kulmala et al., 2012):

$$CS = 4\pi D \sum_j \frac{1}{2} d_{p,j} \beta_m(Kn_j, \alpha) N_j, \quad (1)$$

where D is the H₂SO₄ vapor diffusion coefficient; $d_{p,j}$ is particle diameter; β_m is transitional correction factor for mass flux (Fuchs and Sutugin, 1971) as a function of Kn_j (Knudsen number) and α (mass accommodation coefficient, assumed to be unity in this work), as shown in Eq. (2); N_j is the number concentration of $d_{p,j}$; and the particle diameter is corrected for a growth factor according to T and RH (Laakso et al., 2004).

$$\beta_m = \frac{1 + Kn_j}{1 + 0.377Kn_j + 1.33Kn_j(1 + Kn_j)/\alpha} \quad (2)$$

To quantify if notable growth is to occur, especially for sub-3 nm particles, it is crucial to understand the loss process of fresh particles. Coagulation scavenging of freshly formed particles into pre-existing particles before growing to significant sizes is essential for estimating the concentration of newly nucleated particles at the size of 1.5–2 nm (Kulmala et al., 2001). Aerosol coagulation sink (CoagS) represents this kind of coagulated scavenging characteristics. CoagS (the loss through coagulation among particles) was determined from Eq. (3). Here, K_{ij} is the coagulation coefficient (Kulmala et al., 2001).

$$CoagS = \sum_j K_{ij} N_j \quad (3)$$

Aside from this, the GRs in NPF events were determined with both the appearance time method (including APT- x and APT- y) and the mode fitting method (MOD) to minimize the

uncertainty from calculations (Dada et al., 2020; Kulmala et al., 2012). The detailed approach is shown in the Supplement. The size-segregated GRs were calculated in two size ranges, i.e., sub-3 nm (GR_{<3}) and 3–7 nm (GR_{3–7}), based on the appearance time method, and the 50 % appearance time is fitted by smoothing the normalized concentration time series for the particle of each size bin (Lehtipalo et al., 2014; He et al., 2021a). After determining the 50 % appearance time for each size bin, the GRs were fitted using the linear least-squares method both with time as x and y to compare with each other and minimize the error. They are referred to as APT- x and APT- y , respectively, in this study. The slope of particle size to their 50 % appearance time was regarded as GR using APT- x , which is the traditional way. However, as the particle diameter is exactly measured by our instruments and the 50 % appearance time is the independent variable determined by calculations, we also tried to use the latter as the independent variable to fit the GR. In this case, the GR was determined as the inverse of the fitted slope. The mode fitting (MOD) method fits the particle number size distribution to find the mode diameters at any given time and tracks the evolution of particle sizes. Up to now, there is still a debate about whether to adopt the appearance time method or the mode fitting method for GR calculation, as neither is perfect for calculating GR for ambient observations (Qiao et al., 2021; Deng et al., 2020b). For example, it is difficult to define the accurate mode diameter, especially for sub-3 nm particles when the new particle formation just occurs. Therefore, there could be some underestimation while using the mode fitting method to calculate GR_{<3} (Cai et al., 2022a). Determining the sub-3 nm particle growth can also be difficult for the 50 % appearance time method for similar reasons. Additionally, appearance time method might be more sensitive to other processes as it does not track the growth of a particle or a population (Lehtipalo et al., 2014; R. Cai et al., 2021b; He et al., 2021a). In this study, we report results using both methods to reduce the overall uncertainty of GR calculation and to provide a confidence range of GR. In both cases, the GR is determined from the rate of change in diameter shown as Eq. (4) (Kulmala et al., 2012).

$$GR = \frac{dd_p}{dt} \quad (4)$$

It is worthwhile to note that we corrected the GR obtained from the 50 % appearance time method for the impact of coagulation sink, following Eq. (5) (R. Cai et al., 2021b).

$$GR_{\text{corr,cond}} = GR_{\text{conv}} - \left(CoagS + \frac{CoagSrc}{2N_p} \right) \times \left[\sqrt[3]{(d_p^3 + d_1^3)} - d_p \right] - GR_{\text{coag}}, \quad (5)$$

where the GR_{conv} is the GR calculated from conventional appearance time method (in nm s⁻¹); CoagSrc is the coagulation source, defined as the production rate of the particle size

bin because of coagulation ($\text{cm}^{-3}\text{s}^{-1}$) calculated using the Eq. (6); N_p is the number concentration of particles with the size d_p ; and GR_{coag} is the coagulation growth rate (in nm s^{-1}) from Eq. (7). More specific details can be found in R. Cai et al. (2021b).

$$\text{CoagSrc} = 0.5 \times \iint_{\substack{d_i^3 + d_j^3 \leq d_{p,u}^3 \\ d_{p,1}^3 \leq d_i^3 + d_j^3}} \beta_{i,j} n_i n_j \times d \log d_i \times d \log d_j, \quad (6)$$

$$\text{GR}_{\text{coag}} = \sum_{d_p=d_{\min}}^{d_p=d_p} \left\{ \beta_{p,i} N_i \times \left[\sqrt[3]{(d_p^3 + d_i^3)} - d_p \right] \right\}, \quad (7)$$

The counterbalance of CoagS and GR considerably affects the survival of small clusters (Mahfouz and Donahue, 2021). Survival probability (SP) is utilized to quantify the competition between growth and scavenging mentioned above (Veli-Matti Kerminen, 2002; Kerminen et al., 2005). We defined the $\text{SP}_{1.5-3}$ and SP_{3-7} as the likelihood that the particles can grow from the smaller sizes to the larger sizes (i.e., from 1.5 to 3 and from 3 to 7 nm, respectively) before they are scavenged by coagulation. The SP can be calculated following Eq. (8) (Lehtinen et al., 2007):

$$\text{SP} = \exp \left\{ \frac{d_{p1}}{m-1} \frac{\text{CoagS}}{\text{GR}} \left[\left(\frac{d_{p2}}{d_{p1}} \right)^{1-m} - 1 \right] \right\}, \quad (8)$$

where d_{p1} and d_{p2} are the lower-limit size and upper-limit size, respectively; CoagS is the coagulation sink at the lower limit size; GR is the averaged growth rate in the size range, from both corrected appearance time method and mode fitting method; and m was assumed to be 1.7 according to the measured PNSDs (Lehtinen et al., 2007).

2.2.2 Contribution of HIO₃ to GR and SP

To better understand the role of HIO₃ as an additional GR contributor at two sites, we calculate the condensational GR of HIO₃ and H₂SO₄ during NPF events; the computation criteria are listed as below. The particle growth rate due to HIO₃ concentration was observed to be linear in the CLOUD experiment, shown as Eq. (9), which is fitted at 10 °C (He et al., 2021b):

$$\text{GR}(\text{HIO}_3)_{1.8-3.2} = 10^{\log_{10}[\text{HIO}_3] - 6.75}, \quad (9)$$

where $[\text{HIO}_3]$ is the iodine acid concentration (in molec. cm^{-3}) and $\text{GR}(\text{HIO}_3)_{1.8-3.2}$ is the growth rate of 1.8 to 3.2 nm particles (in nm h^{-1}). However, the size range of sub-3 nm particles used in this study (1.5 to 3 nm) slightly differs from 1.8 to 3.2 nm, and this formulation does not provide the growth rates of 3 to 7 nm particles. Additionally, as the temperature in summer seasons in both Beijing and Nanjing (around 22 to 36 °C) is much higher than 10 °C, additional temperature correction is needed. In

this study, we adopt the equation provided by Nieminen et al. (2010) for these corrections:

$$\text{GR}'(\text{HIO}_3) = \frac{\Delta d_p}{\Delta t} = \frac{\Delta d_p \text{HIO}_3 \alpha_m m_v}{2 \rho_v d_v} \cdot \sqrt{\frac{8kT}{\pi m_v}} \cdot \frac{1}{\left[\frac{2x_1+1}{x_1(x_1+1)} - \frac{2x_0+1}{x_0(x_0+1)} + 2 \ln \left(\frac{x_1(x_0+1)}{x_0(x_1+1)} \right) \right]}, \quad (10)$$

where the subscript “v” refers to HIO₃. Additionally, x_0 and x_1 are the ratios of the diameter of HIO₃ molecule divided by the particle diameter at which the initial growth occurs (e.g., 1.5 or 1.8 nm) and particle diameter at which the particles grow to (e.g., 3 or 3.2 nm), respectively. Two sets of growth rates were calculated using this equation: (i) the first set utilized the measured ambient temperature at the given growth period of NPF events with 1.5 to 3 or 3 to 7 nm as the growth ranges, and (ii) the second set calculated the growth rates at 10 °C with 1.8 to 3.2 nm as the growth range (the same as at CLOUD). The ratios of the growth rates calculated by (i) and (ii) therefore give the correction factors that can be applied to Eq. (9) to correct the temperature and size differences. The correction factors, determined by analyzing temperature measurements at two sites and selected size ranges on NPF event days, remained consistently close to 1 (as shown in Fig. S2 for more detailed information). This suggests that the variations in size range and temperature between the CLOUD measurements and our field observations are minimal.

To quantify the growth rates of particles with a mean diameter from around 1 to 7 nm in Nanjing, the negative ion number size distribution collected by NAIS was utilized. However, it is extremely difficult to use the NAIS to capture sub-3 nm particle growth rates as the limited atmospheric ions are mostly captured by larger particles in polluted urban environments, thus leaving the sub-3 nm particle growth undetectable (see Supplement for details). Therefore, in all NPF cases that occurred at the SORPES station, the contribution of gaseous iodine acid to sub-3 nm growth is only quantified by comparing its contribution with that of sulfuric acid during the same event, since H₂SO₄ is believed to be the significant contributor to particle initial growth in sub-3 nm range (Deng et al., 2020b).

$$\text{GR}(\text{H}_2\text{SO}_4) = \left(2.68 \times d_p^{-1.27} + 0.81 \right) \times \left([\text{H}_2\text{SO}_4] \times 10^{-7} \right) \quad (11)$$

The H₂SO₄ contribution to GR is calculated as a first-order approximation independent of temperature as Eq. (11) (Stolzenburg et al., 2020), where $d_p = \frac{d_{p\text{initial}} + d_{p\text{final}}}{2}$ (in nm), and the initial and final subscripts refer to the particle diameter at the beginning and the end of the growing process, respectively. $[\text{H}_2\text{SO}_4]$ is the gas-phase H₂SO₄ concentration (in molec. cm^{-3}). It should be noted that H₂SO₄ does not

dominate the initial growth process alone as other organic species may make some contribution as well. Therefore, in this study, the results calculated at SORPES are disadvantaged compared to the BUCT/AHL data using directly measured GRs. This part of the results should be considered a compromise due to the absence of direct measurements.

We define SP_{tot} as the particle survival probability calculated using the measured GRs (in Beijing) or the expected growth rate considering growth contributions from both H₂SO₄ and HIO₃ (in Nanjing). In order to quantify the SP enhancement by HIO₃, we further define SP₁, which represents the calculated survival probability using GRs after deducting the growth contribution from HIO₃. Therefore, the enhancement factor (EF) of SP can be represented as

$$EF = \frac{SP_{\text{tot}}}{SP_1} - 1. \quad (12)$$

2.2.3 Iodic acid (HIO₃) precursor proxy

In order to investigate the source of gaseous HIO₃ at both sites, a daytime proxy formula is built to describe the precursor level of measured HIO₃, which is as follows:

$$\text{Proxy}_{\text{pre}} = \frac{[\text{HIO}_3] \times \text{CS}}{\text{UVB}}. \quad (13)$$

Equation (13) is derived by assuming the HIO₃ concentration to be at a pseudo-steady state (the production rate equals to the loss rate). Based on current knowledge about HIO₃ formation pathways, the proxy is not intended to elucidate the composition of species serving as HIO₃ precursor or the related reactions. Instead, it considers the photochemical reaction as the daytime formation pathway and condensation onto pre-existing aerosol particles as the only sink for gaseous HIO₃.

3 Results and discussion

3.1 Overview of the measurement

The measurement overviews in both Beijing and Nanjing are presented in Fig. 1, including the time series of *T*, O₃, HIO_x, and H₂SO₄ concentrations, as well as the frequency of NPF events in each month. It should be noted that each point on time series panels refers to daytime mean value. In this work, daytime duration is defined between 08:00 and 16:00 local time (LT, UTC+8) considering the preferred time window of NPF events in China (Kulmala et al., 2021), as shown in Fig. S3.

In Fig. 1a, d, it is obvious that the seasonal patterns of *T* and O₃ are similar during measurement periods in both sites, i.e., both peak in the summer. The O₃ levels are roughly the same at both sites, and the maximum values of daily mean *T* are both over 35 °C, though the lowest *T* (about 1 °C) in Nanjing is significantly higher than that in Beijing (about −12 °C).

H₂SO₄ concentration is slightly lower in cold seasons (Fig. 1b, e). H₂SO₄ concentration exceeds 10⁷ cm^{−3} only on a few days in Beijing, whereas it is a common phenomenon in Nanjing daytime. Besides H₂SO₄, we report the first long-term measurement of HIO_x in urban environments continued from earlier sparse measurements (He et al., 2021b). The calibrated HIO_x concentration is above the detection limit during almost the entire measurement periods, indicating a clear presence of HIO_x in inland cities. The HIO₃ concentration was between 10⁵ and 10⁶ cm^{−3} for most of the time except for winter months; it sporadically approaches or is higher than 10⁶ cm^{−3} in warm months. On the other hand, iodic acid, HIO₂ is less abundant than HIO₃ at both sites with a general concentration at around 10⁴ cm^{−3} and a maximum concentration approaching 10⁵ cm^{−3} in the summer. The results indicate that the H₂SO₄ concentrations are generally higher than that of iodine oxoacids at both sites. The ratios of HIO₃ to H₂SO₄ at both sites differ so slightly, with about 10 % in Beijing and 9 % in Nanjing, respectively. As for the two iodine oxoacids (HIO₃ and HIO₂), daytime mean concentration of HIO₃ is more than an order of magnitude higher than HIO₂. The order-of-magnitude-lower HIO₃ concentration compared with H₂SO₄ in summer at both sites is consistent with that in the Finnish subarctic boreal forest (Jokinen et al., 2022).

The frequencies of NPF events varied significantly, from none to more than 75 % of the days in each month during the measurement period. The occurrence of NPF events in China is favored by various meteorological factors (Qi et al., 2015; Zhou et al., 2021; Chu et al., 2019). However, the influences can be quite uncertain and complex because of different season and the location of measurement site. Take temperature for an example; on the one hand, warm temperatures enhance the abundance of biogenic and anthropogenic volatile organic compound emissions, as well as their oxidation processes (Paasonen et al., 2013, 2018; Nie et al., 2022; Ehn et al., 2014). On the other hand, the warm temperature also reduces the stability of embryonic clusters, thus reducing nucleation and subsequent growth rates (Kürten et al., 2016). Besides meteorological conditions, vapor condensation sink (CS) and particle coagulation sink (CoagS) have negative effects on the NPF frequency (Kalkavouras et al., 2017; Bousiotis et al., 2021; Wehner et al., 2007). Decreased CS and/or CoagS will lead to faster nucleation and subsequent growth (as scavenging of nucleating and condensable vapors is less effective) and higher survival probability through the growth processes during NPF events (as the scavenging of clusters and small particles is less effective). As expected, the concentration of gaseous H₂SO₄ is notably correlated with NPF frequency, as H₂SO₄ is the most important compound to form initial clusters and one of the main contributors to the growth of newly formed particles (Nieminen et al., 2010; Kirkby et al., 2011). During this measurement, the ratio of GR_{1.5–3} contributed from H₂SO₄ to measured GR calculated from MOD is about 72.4 % (shown in Table S4).

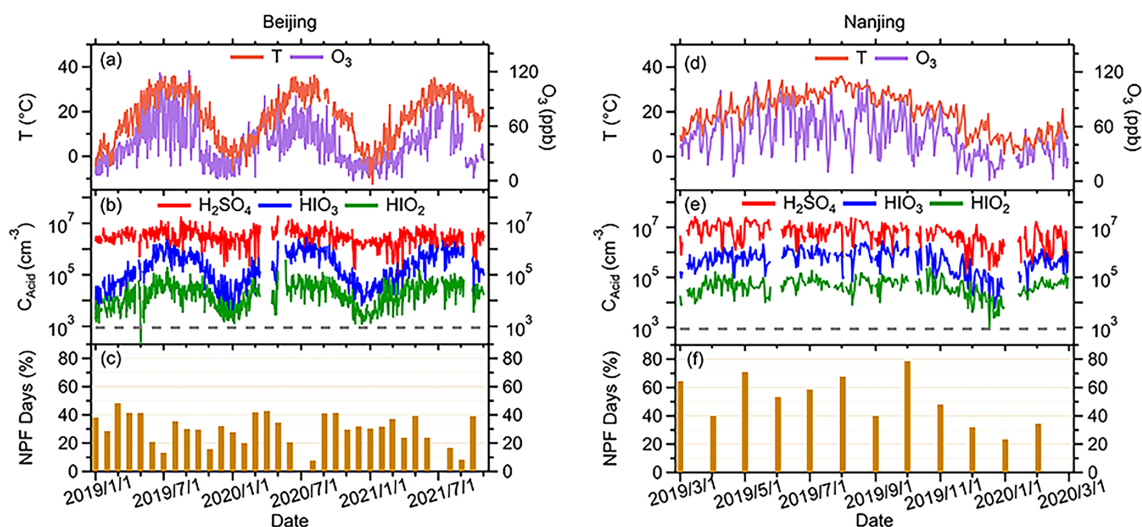


Figure 1. Time series of parameters from 1 January 2019 to 31 October 2021 in Beijing (a–c) and from 1 March 2019 to 29 February 2020 in Nanjing (d–f). (a, d) Temperature and ozone. (b, e) Sulfuric acid and iodine oxoacid concentrations. The dashed grey line represents the detection limit of instruments (875 cm^{-3}). (c, f) The frequencies of new particle formation events in each month. Time resolution for all the presented data is 1 d and the environmental parameters and vapor concentrations are averaged daytime (08:00 to 16:00 LT) mean.

As depicted in Fig. 1c and f, the frequencies of NPF for each month at two sites are quite different, since environments are chemically complex and diverse with many aforementioned factors influencing NPF. Generally, NPF events are more likely to occur in the spring and winter, with the lowest frequency in summer at BUCT station in Beijing, consistent with other reports (Wu et al., 2007; Deng et al., 2020b). Different from Beijing, there are fewer NPF events in the winter than in the summer at SORPES station, which is in line with a long-term measurement conducted at the same site (Qi et al., 2015). It could be attributed to the lowest H_2SO_4 concentration in cold season, which was found to be the main driver for NPF events in polluted megacities in China (Yao et al., 2018). Another explanation may be that the high CS in the winter daytime (Qi et al., 2015) suppresses the NPF events. It should be noted that the particle formation mechanism in Nanjing is yet to be revealed and NPF intensity could be reduced if DMA is limited in Nanjing.

3.2 Characteristics of acid concentrations

3.2.1 Seasonal variation

To better understand the roles of the studied acids in NPF, we further present the seasonal variation in H_2SO_4 , HIO_3 and HIO_2 concentrations in Fig. S4. It depicts the monthly statistics of H_2SO_4 and HIO_x at the two sites with different shading indicating the seasons. H_2SO_4 and HIO_x concentrations in Nanjing are always higher than those in Beijing except for H_2SO_4 concentrations in the winter. We speculate that the generally higher acid concentrations in Nanjing are caused by stronger solar radiation at latitude of $32^\circ 07' \text{ N}$ in Nanjing, compared with $39^\circ 56' \text{ N}$ in Beijing. On the other

hand, the reason for higher wintertime H_2SO_4 concentrations in Beijing is likely the higher SO_2 and more frequent sunny weather during the winter in Beijing (Wang et al., 2018); further discussion is provided in the Supplement. At both sites, the seasonal pattern of H_2SO_4 is not very strong (Deng et al., 2020b; Petäjä et al., 2009). H_2SO_4 concentrations are higher in the spring and autumn, lower in the summer, and lowest in the winter. This variation in H_2SO_4 in different seasons is determined by both its source and sink. Winter is characterized by the weakest solar radiation and the heaviest particle pollution, which collectively result in lowest H_2SO_4 levels, whereas lower SO_2 concentrations in summer could limit H_2SO_4 formation.

The HIO_3 concentrations measured at the two sites are significantly lower, approximately 2 orders of magnitude lower than that at the pristine coastal site (e.g., in Mace Head). Measurements at Mace Head indicate that HIO_3 concentrations are frequently above 10^7 cm^{-3} with some days exceeding 10^8 cm^{-3} in September. The concentrations of atmospheric iodine at coastal sites are normally higher due to active biogenic emissions of iodine-containing precursors from marine algae (O'Dowd et al., 2002). On the other hand, HIO_3 concentrations in Beijing and Nanjing are comparable to that in Helsinki, Finland. Measurements at SMEAR III station, an urban site located at the University of Helsinki show HIO_3 concentrations at around 10^6 cm^{-3} when the wind is coming from land for most times in August and HIO_3 concentrations exceed 10^7 cm^{-3} when air masses have marine origin (Thakur et al., 2022; He et al., 2021b). Another long-term observation conducted at SMEAR I station (Jokinen et al., 2022), a subarctic boreal forest site, shows HIO_3 concentrations often at around 10^5 cm^{-3} from April

to November 2019 (summer and autumn) with occasional peaks exceeding 10^6 cm^{-3} in late August. HIO_x concentrations at AHL/BUCT station depict a distinctly unimodal pattern in a year cycle with the highest values in July, increasing from January and decreasing to December. However, seasonal variations of HIO_x are slightly different at SORPES, as there are similar levels of HIO_x throughout the summer in 2019, reaching a seemingly steady daily maximum. HIO₃ concentration measured from August to September in 2018 over the central Arctic Ocean increases significantly from summer towards autumn (Baccarini et al., 2020), which is different from the results in both Beijing and Nanjing, due to significantly different environments and iodine sources.

3.2.2 Diurnal pattern

Though the HIO₃ concentrations are different in the four seasons, the diurnal patterns are similar throughout the year (Fig. 2). Daily trends of both median H₂SO₄ and HIO_x concentration are strongly connected with diurnal cycle. The concentration of HIO_x increases at the same time as H₂SO₄, i.e., both HIO_x and H₂SO₄ rise in the early morning and peak from noon to afternoon. The clear diurnal pattern of H₂SO₄ has been attributed to photochemical activities (Lu et al., 2019; Yang et al., 2021; Petäjä et al., 2009). Hydroxyl radical (OH) is the most important oxidant for sulfur dioxide (SO₂) to form daytime H₂SO₄ (Guo et al., 2021; Yang et al., 2021). Therefore, the diurnal pattern of H₂SO₄ would be affected by its precursors (e.g., SO₂ and OH in daytime). Higher HIO_x concentrations in the daytime and the absence of their nocturnal maxima suggest that the main source of HIO_x is also photochemical oxidation of iodine precursor vapors. As depicted in Fig. 2, this pronounced diurnal variation in HIO_x levels is consistently observed at both sites throughout the entire measurement period, regardless of the season. The peak concentrations of HIO_x consistently exceed the minimum levels by a factor of approximately 1 order of magnitude, with this difference being particularly significant, especially for HIO₃ during summer. The distinct variation from day to night suggests that HIO_x formation is primarily occurring in situ, rather than being transported from other regions. Although the diurnal patterns of H₂SO₄ and HIO₃ are alike, the occurrence of HIO₃ daytime maximum is on average later than that of H₂SO₄ at both sites (Fig. 2). This phenomenon is pronounced regardless of season at both sites, with the daily maximum of H₂SO₄ appearing around 1–2 h earlier than that of HIO₃. It implies that although these two acids form during daytime through photochemical pathways, the limiting factors for their productions can be different. At the SORPES station, for instance, the diurnal cycle of H₂SO₄ follows that of radiation. In summer, however, owing to the effectiveness of long-term emission reduction, SO₂ concentrations can be low enough to limit the production of H₂SO₄ at SORPES (Ding et al., 2019), so the daytime peaks of H₂SO₄ tend to occur when SO₂ reached its daily maximum (Yang et

al., 2021). On the other hand, little is known about the diurnal patterns of HIO_x in urban environments. It was demonstrated in chamber experiments that HIO_x can be formed by oxidation of oxidized iodine species with ozone in the absence of HO_x (He et al., 2021b), and the I₂O₂ + O₃ reaction was recently found to be the critical step for the HIO₃ formation (Finkenzeller et al., 2023). The diurnal patterns show that the maximum of daytime HIO₃ concentrations mimics that of O₃ in all seasons, indicating that O₃ may influence terrestrial HIO₃ formation. However, the role of O₃ in HIO₃ formation can be multifaceted and warrants more thorough discussion in the future studies with extensive measurements of other iodine compounds in inland regions, especially urbanized areas. On the one hand, chamber studies have shown the direct involvement of O₃ in the formation of HIO₃ precursors in less chemically complex scenarios. On the other hand, O₃ has been proved to simulate the release of iodine compounds in marine environments from surface seawater (Carpenter et al., 2013), and similar processes are likely to occur in urban environments as well. Additionally, temperature may also have favorable impacts on both the formation of HIO₃ and the release of iodine precursors, which will be discussed in the next section.

Moreover, CS in Nanjing shows an opposite profile to *T* and O₃, whereas it keeps almost the same trend as that of Nanjing but fluctuates a little during the day in Beijing spring and winter, which shows median values only in 2019. In summary, the diurnal patterns shown in Fig. 2 suggest that stronger solar radiation coupled with higher mixing ratio of O₃ and higher *T* are likely the factors favoring the formation of acids, and the low CS at noon is preferred for the survival of acid vapor. Additionally, the diurnal variation in HIO_x at BUCT shows stronger seasonality with its highest values at around noon in the summer. The maximum concentrations at spring and autumn are similar, while the maximum concentrations in the winter are roughly an order of magnitude lower. At SORPES, HIO_x reaches similar levels in the spring, summer, and autumn, but its concentration is lower in the winter. Consistently, the diurnal maximum HIO₃ concentration in summer approaches 10^6 cm^{-3} at both sites.

3.2.3 Iodine sources

In order to investigate the source of HIO_x in urban environments, we further conduct cluster analysis of the air mass backward trajectories of the AHL/BUCT station in warm seasons (from May to September in this study). The HIO₃ precursor proxy calculated from Eq. (13) based on the measurement results at BUCT/AHL station is classified into four levels, as shown in Fig. S5 (see Sect. S4 for more details). High precursor levels are mainly associated with air masses originating from the south and southeast, whereas lower iodine precursor concentrations are associated with northern air masses. It implies that marine iodine sources could be important for the AHL/BUCT station due to long-range trans-

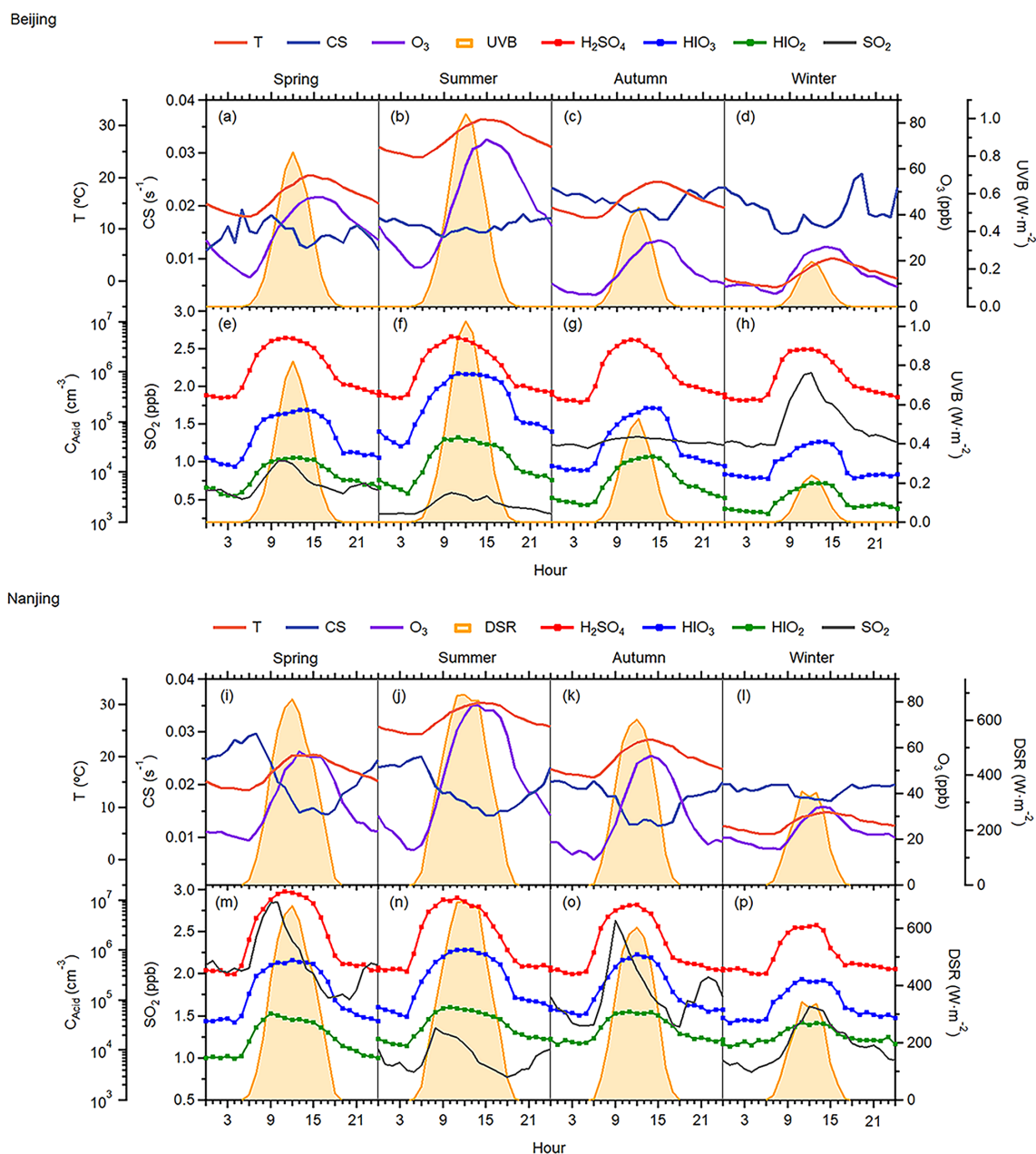


Figure 2. Diurnal variations in median value of O₃, *T*, and CS in the four seasons are shown in the first row (Beijing, **a–d**) and third row (Nanjing, **i–l**), and the diurnal variations in median SO₂, H₂SO₄, and HIO_x concentrations in the four seasons are shown in the second row (Beijing, **e–h**) and fourth row (Nanjing, **m–p**). The columns are profiles in spring, summer, autumn, and winter, respectively. The diurnal patterns of UVB were plotted in every panel to better compare them with other factors.

port. Additionally, the air mass travels from northern wind may also carry substantial precursors of HIO₃, indicating the potential terrestrial sources of iodine. Therefore, both marine (O'Dowd and Hoffmann, 2005; Carpenter et al., 2021) and terrestrial precursors such as soil fumigants (Li et al., 2014; Wang et al., 2017) may contribute to the HIO₃ formation at the AHL/BUCT site.

Both seasonal variation and diurnal patterns show the lowest concentration of HIO_x in winter when the impact from

residential coal burning and fossil fuel combustion power plants in Beijing is the largest. It implies that HIO_x concentration is not promoted by pollution in the cold season. The negative correlation between HIO₃ and BC shown in Fig. S6 further demonstrates the irrelevance of winter pollution on the HIO₃ in Beijing. A previous 2-year measurements conducted in Beijing show that high loadings of particulate organic iodine compounds (OICs) occurred in the heating season, and HOI was thought to be the key oxidant to

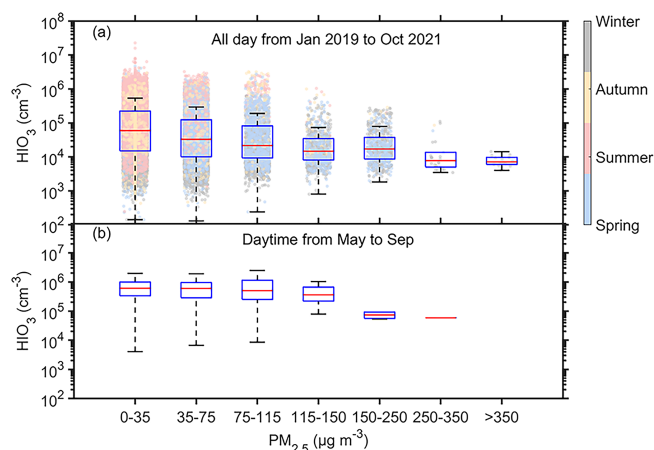


Figure 3. HIO_3 concentration in different $\text{PM}_{2.5}$ level bins. (a) Data from the whole campaign colored by the seasons in Beijing and (b) data for the daytime from May to September (warm seasons) in Beijing.

form the OICs (Shi et al., 2021). The different seasonal distribution between gaseous HIO_x in this study and particle-phase OICs indicates potentially different iodine sources of gaseous and particulate phases, which warrants further investigation. Figure 3a presents HIO_3 in different $\text{PM}_{2.5}$ ranges and shows lower HIO_3 concentrations when $\text{PM}_{2.5}$ increases. $\text{PM}_{2.5}$ measurements in the Beijing–Tianjin–Hebei region (2013 to 2020) show obvious seasonal characteristics with the lowest concentrations in summer and highest concentrations in winter (Yang et al., 2022). This phenomenon should be attributed to the inherently independent seasonality of these two constituents instead of any correlation. If $\text{PM}_{2.5}$ is a source of gaseous iodine species, HIO_3 concentrations should be higher in winter months, which is not the case. Additionally, summertime HIO_3 concentrations in different $\text{PM}_{2.5}$ concentration bins have no difference (Fig. 3b), which further indicates that HIO_3 is not correlated with the particulate matter pollution in Beijing. Furthermore, the results in Fig. S7 demonstrate that $\text{PM}_{2.5}$ pollution does not play a conclusive role in HIO_3 production, especially with the seasonal influence excluded.

There is no definite evidence to justify whether marine or land sources could better explain our observation of HIO_3 concentration in Beijing. In the marine environments, the rapid reaction of sea surface iodide with O_3 is believed to be the largest global source of iodine species in the forms of molecular iodine, I_2 , and hypoiodous acid, HOI (Carpenter et al., 2021, 2013), which in turn contributes to the formation of HIO_x (Finkenzeller et al., 2023; He et al., 2021b). However, the photolysis lifetimes of HOI (~ 140 s) and I_2 (~ 10 s) or biogenic volatile iodocarbons (e.g., CH_2I_2 (~ 5 min)) are too short to contribute to the formation of HIO_x in Beijing and Nanjing considering the long-range transportation (Saiz-Lopez et al., 2012). Another iodine-containing species,

methyl iodide (CH_3I), has a longer lifetime of about 5 d, which may potentially go through the long-range transportation and eventually reach inland cities. CH_3I is dominantly formed from photochemical processes in the marine surface (Moore and Zafiriou, 1994) and additionally also from dust-stimulated abiotic emission (Williams et al., 2007). CH_3I concentration was shown to be correlated with surface seawater temperature (SST) in marine boundary layer air at mid-latitude (Yokouchi et al., 2008). Others reported the opposite results in the Yellow Sea and the East China Sea during summer (Li et al., 2021) and the reason may be that higher surface water temperature also accelerates the chemical loss of CH_3I from the seawater and atmospheric CH_3I is readily photolyzed. Long-term variations of atmospheric CH_3I at several sites show that SST near each site cannot fully explain the variation of observed CH_3I concentrations (Yokouchi et al., 2012). Other factors, such as acidification, i.e., pH conditions, mineral dust deposition, dissolved organic carbon (DOC) concentration (Li et al., 2021), and ferric ion (Fe^{3+}) concentration (Chen et al., 2020) in seawater could also contribute to the emission rate of CH_3I .

Apart from marine sources, terrestrial sources of CH_3I , including most rice paddies (Redeker et al., 2000), terrestrial biomes (Sive et al., 2007), minor wetlands (Dimmer et al., 2001), and biomass burning (Andreae et al., 1996), were also proposed. High concentrations of CH_3I at two inland sites in Japan indicate the greater importance of terrestrial sources in the summer compared to oceanic sources (Yokouchi et al., 2008). As CH_3I emission from rice paddies is positively correlated with temperature (Redeker and Cicerone, 2004; Redeker et al., 2000), CH_3I emission is likely to be stronger in the summertime. This is consistent with higher concentrations of HIO_x in Beijing and Nanjing, as shown in Figs. 1, 2, and 4. Moreover, experiments show that CH_3I emission under dark incubation was much lower than that under light incubation, and CH_3I production under visible light conditions is lower than that under natural light (Li et al., 2021). Those results indicate that ultraviolet light promotes the production of CH_3I (Chen et al., 2020; Li et al., 2021) as well as its photochemical oxidation. This is consistent with our observation that HIO_x is only formed in the daytime (Fig. 4).

The relative importance of terrestrial and marine iodine sources may vary widely with local meteorological factors and the transportation of air masses. Future efforts are needed to verify the composition and distribution of HIO_x precursors in polluted environments.

3.2.4 Formation of HIO_3 in urban environments

Quantum chemical methods and laboratory experiments have both been carried out to investigate the formation mechanisms of HIO_3 . Previous studies using quantum chemical calculations have proposed two possible formation pathways of HIO_3 . Iodine monoxide (IO) was proposed to react with HO_2 radical to yield HIO_3 (Drougas and Kosmas, 2005). The reac-

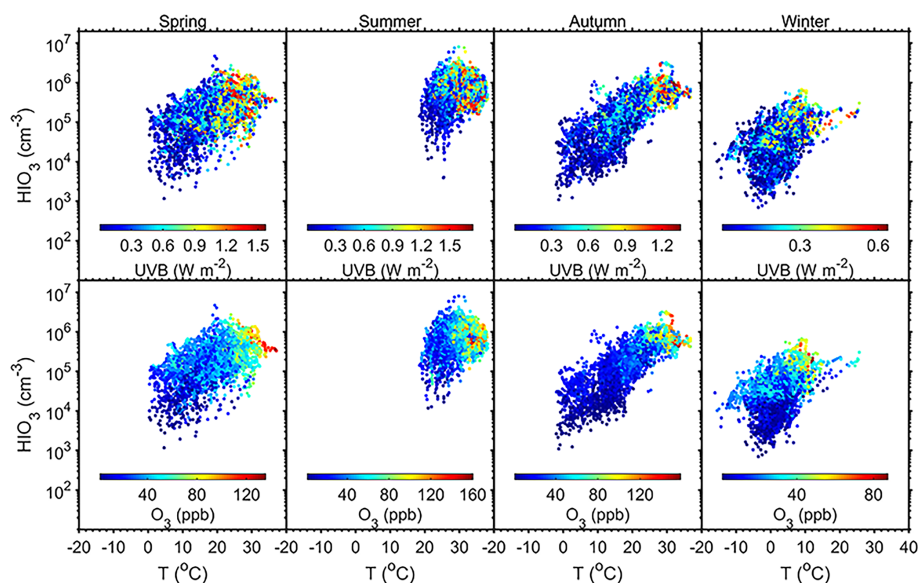
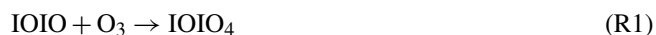


Figure 4. Influences of T , UVB, and O₃ on HIO₃ concentration in the daytime (08:00–16:00 LT) in Beijing. The analysis is separated into the four seasons.

tion between iodine dioxide (IOI) and OH radical was also suggested to produce HIO₃ (Plane et al., 2006). Laminar-flow reactor experiments have also been carried out to investigate the formation mechanisms of HIO₃ from I₂ (He, 2017). With the illumination of green fluorescent lamp, I₂ was efficiently photolyzed while O₃ photolysis was restricted, and thus there was no known source of HO_x. Surprisingly, a significant amount of HIO₃ was formed under essentially HO_x-free conditions. To rule out a potential unknown OH source in the flow reactor, different OH scavengers (methane, sulfur dioxide, cyclohexene, and acetic acid) were injected, but the production of HIO₃ remained. Iodine atoms or iodine oxides were proposed to be the reactants with ozone and water to produce HIO₃. Studies from the CLOUD experiments suggest that iodoxy hypoiodite (IOIO) could be efficiently converted into HIO₃ via Reactions (R1) and (R2) (Finkenzeller et al., 2023), which successfully explain earlier laboratory and field observations (Sipilä et al., 2016; He et al., 2021b). These results align with our observations at the AHL/BUCT station. UVB is an indication of light intensity and influences the production of I atoms from the photolysis of I₂ and CH₃I. The produced iodine atoms react with O₃ and further drive gaseous iodine chemistry (Saiz-Lopez et al., 2012). Figure 4 depicts the correlation of UVB, O₃, and temperature. Although the correlation between HIO₃ concentration and air temperature is not very strong, high HIO₃ concentrations appear when both the UVB and O₃ mixing ratios are high. This is consistent with the fact that both solar radiation and O₃ are required to initiate the iodine emission and iodine photochemistry.



3.3 Iodic acid enhances the particle survival probability

Statistical results show that NPF events occur frequently at both sites throughout the measurement periods. Whether freshly nucleated particles can contribute to cloud condensation nuclei and hence impose influence on climate and human health depends largely on how fast they grow into larger particles and survive from coagulation scavenging by pre-existing aerosols, which is more efficient for smaller particles. The GR of newly formed particles is therefore central for sub-10 nm particle lifetimes in ambient environments. Earlier studies have linked some dimensionless parameters L or L_{Γ} (McMurry et al., 2005; Kuang et al., 2010; Cai et al., 2017b) to justify the occurrence of NPF and described the competition between aerosol surface area and condensable vapors during the growth period. Recently, a dimensionless survival parameter P (Kulmala et al., 2017) was proposed as the ratio of CS' (CS/10⁻⁴ s⁻¹) to GR' (GR/1 nm h⁻¹). From this ratio, P shows the competition between the possibility of being cleared and growing to survive. When P is below 50 in clean environment or 100 in polluted urban cities, the SP of the sub-3 nm particles is agreed with the atmospheric observations (Kulmala et al., 2017). As shown in Fig. S8, the median P is about 50 for the sub-3 nm particles, whereas the median P value is about 20 for 3–7 nm particles in the NPF events at the AHL/BUCT station. That means the growing particles in those days preferred to survive and thus showed us clear new particle formation and further growth.

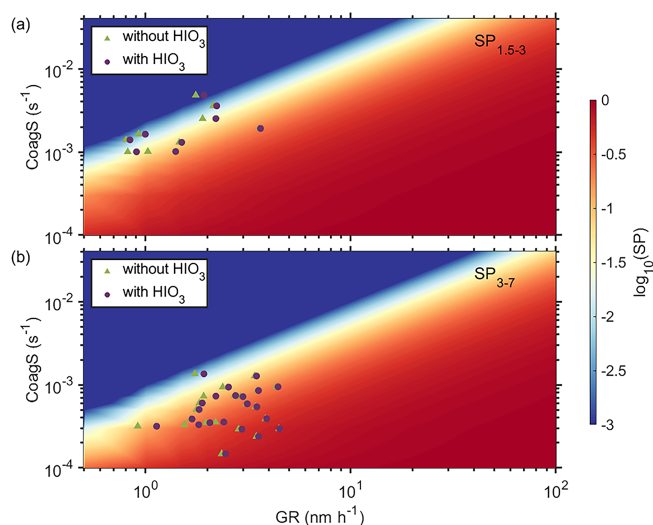


Figure 5. The effect of coagulation sink and growth rate on particle survival probability for 1.5–3 nm (a) and 3–7 nm (b) particles, respectively.

As shown in Eq. (8), the impact of GR on survival of new particles is not linear and a small enhancement on GR could result in much larger enhancement in particle survival probability (M. Cai et al., 2021). It also means that the SP of these newly formed particles exhibits a substantial variability, spanning more than 3 orders of magnitude, as illustrated in Tables S2–S4. To further illustrate the nonlinear response of particle SP, we plot the logarithmic value of SP ($\log_{10}(\text{SP})$) as a function of CoagS and GR from 1.5 to 3 nm (Fig. 5a) and from 3 to 7 nm (Fig. 5b), respectively. The value of SP is extremely sensitive to both CoagS and GR. Under the typical CoagS (around 0.0025 s^{-1}) at both sites, the SP could be enhanced by more than 2 orders of magnitude when GR is varied from 1 to 10 nm h^{-1} . Increased GR caused by additional condensing vapors enables faster growth, which in turn facilitates the survival of sub-10 nm particles from coagulation scavenging (Kuang et al., 2012). This effect is especially important for sub-3 nm particles as they are the most susceptible and are easily lost to large pre-existing particles.

We present case studies of several consecutive NPF events at both sites in Fig. 6. At the AHL/BUCT station, NPF events occurred from 25 to 29 May 2021 due to favorable meteorological conditions, except for one undefined day (27 May 2021) when no obvious growth was observed. On this undefined day, the UVB in the daytime was low and the intensity was fluctuating due to cloudiness. Both of these conditions, as well as the higher CS, suppressed the NPF (Kerminen et al., 2018; Deng et al., 2020a; R. Cai et al., 2021a). On the other hand, both T and O_3 , as well as UVB, increased from around 06:00 LT in the morning on the NPF event days, with decreasing RH. The averaged concentrations of H_2SO_4 and HIO_3 in the particle growth periods from 1.5 to 7 nm on event days and from 08:00 to 10:00 LT on the other days were

summarized in Table 1. The ratio of HIO_3 concentration to H_2SO_4 was about 5 % in the first 3 d and more than 10 % in the next 2 d, likely due to higher O_3 concentrations, which contributes to the emission of iodine precursors.

Tables S2–S4 and S5–S7 summarize the HIO_3 contribution to GR and SP in the particle size range of 1.5–3 and 3–7 nm, respectively. To account for the uncertainties in the GR and SP calculations, the measured GR values are calculated using three methods, namely the APT- x , APT- y and the mode-fitting (MOD) methods (see Sect. S5, Fig. S9). We present the results from MOD methods in the main text to keep consistency with earlier studies (Deng et al., 2020b; Qiao et al., 2021). Only events with clear growth were reported in this study to reduce systematic uncertainties resulting from the GR calculation. We also provide the results from the APT- x and APT- y methods in the Supplement for completeness. The results in Tables S2–S4 show that the contributions of HIO_3 to $\text{GR}_{<3}$ on 25 and 26 May were lower than 5 %, whereas the contribution was about 10 % on 29 May. The $\text{SP}_{1.5-3}$ enhancement from HIO_3 is much stronger on 29 May, even reaching 40.5 %. Although the contribution of HIO_3 to $\text{GR}_{<3}$ on 21 June 2021 is almost identical to that on 29 May 2021, SP enhancements on 21 June 2021 are 2.5 times larger. This is a result from the 5 times CoagS on 21 June 2021. This suggests that in polluted environments with higher CoagS, such as Beijing, SP enhancement can be more sensitive to GR enhancement. Results in both Figs. 7 and S10 show that the median contribution of HIO_3 to the GR of particles in the 1.5–3 nm size range is 7.4 % using the MOD method, whereas the contribution is only around 3 % and 2 % using the APT- x and APT- y methods, respectively. This resulted from the difference in the measured GR calculated using either the APT or the MOD methods. This further translates into 40.5 %, 10.8 %, and 4.1 % SP EF using the MOD, APT- x , and APT- y methods, respectively. Despite the uncertainty in the measurement GR calculation, the EF of HIO_3 to sub-3 nm particle SP is clear: in 55.6 %, 33.3 %, and 25.0 % of the events HIO_3 enhances particle SP by more than 30 %, using MOD, APT- x , and APT- y methods, respectively.

Additionally, we show three consecutive NPF events observed from 16 to 18 August 2019 at the SORPES station, Nanjing. These events feature high acid concentrations, O_3 mixing ratios, and strong light intensities, as well as low RH and CS. No nucleation mode particle burst was observed on August 20, probably owing to decreased H_2SO_4 concentration. Compared to the cases in Beijing, the concentrations of O_3 and acids are twice as high at the SORPES station due to geographical and seasonal differences (Table 1).

From June to December 2019, there are 23 NPF events recognized at the SORPES station. Due to the detection limitation of the instruments at SORPES, the sub-3 nm particles were not clearly measured, which in turn poses challenges to get the measured GR through the 50 % appearance time method or the mode fitting method. The statistics are depicted in a different way from that of the AHL/BUCT

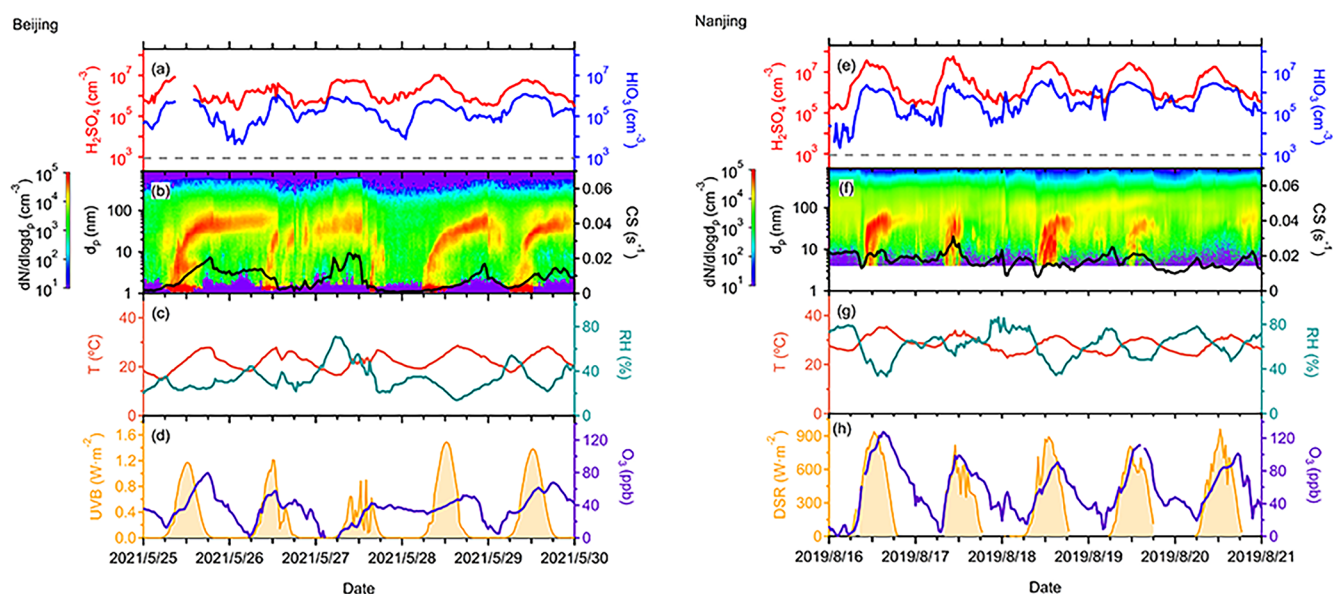


Figure 6. Cases of consecutive NPF events in Beijing (a–d) and Nanjing (e–h) sites. Acid concentrations are shown in the first row; particle number size distribution and CS are shown in the second row; and meteorological factors, such as T , RH, UVB, and O₃ concentrations are also presented in the third and fourth rows. The measurement of acids in the Beijing site was unavailable for a short period on 25 May (a).

Table 1. Environmental factors and acid concentrations shown in Fig. 5.

Site	Date (yyyy/m/dd)	Start time (LT)	End time (LT)	H ₂ SO ₄ (cm ⁻³)	HIO ₃ (cm ⁻³)	CS (s ⁻¹)	T (°C)	RH (%)	UVB/DSR (W m ⁻²)	O ₃ (ppb)
Beijing	2021/5/25	06:50:00	09:23:00	3.96×10^6	2.03×10^5	0.0046	18.5	26	0.20	25.68
	2021/5/26	09:20:00	10:48:36	8.01×10^6	4.90×10^5	0.0105	24.25	32	0.84	47.82
	2021/5/27	08:00:00	10:00:00	1.66×10^6	5.41×10^4	0.0222	19.6	59	0.45	11.17
	2021/5/28	06:00:00	08:15:00	5.35×10^6	7.21×10^5	0.0018	20.35	34	0.10	31.51
	2021/5/29	06:20:00	09:38:44	3.89×10^6	4.99×10^5	0.0040	19.4	50	0.25	31.24
Nanjing	2019/8/16	10:22:21	14:59:49	2.03×10^7	1.40×10^6	0.0200	33.23	40.69	858	105.38
	2019/8/17	08:04:22	11:10:40	4.27×10^7	1.79×10^6	0.0268	32.02	56.43	525	75.27
	2019/8/18	10:17:53	17:18:42	2.06×10^7	2.20×10^6	0.0134	30.93	39.52	705.1	81.09
	2019/8/19	08:00:00	10:00:00	1.35×10^7	2.48×10^6	0.0164	27.99	61.71	419.7	58.72
	2019/8/20	08:00:00	10:00:00	1.07×10^7	2.12×10^6	0.0154	27.4	67.08	458	48.26

(see the Supplement for further details). Briefly, the contribution of HIO₃ and H₂SO₄ to sub-3 nm particle GR in NPF events are quantified based on Eqs. (9), (10), and (11). This is based on the observed consistency between the gaseous H₂SO₄ concentration and its significant contribution to the sub-3 nm particle growth rate in Beijing (Deng et al., 2020b). The SP enhancement is further calculated based on Eq. (12). Consistent with the observation at the AHL/BUCT station, the concentration of gaseous HIO₃ in Nanjing is lower than H₂SO₄ throughout the measurement period, accounting for 10%–20% of concentration (Fig. 1e). However, the average HIO₃:H₂SO₄ ratio (16.8%) is higher than that in Beijing (10.7%).

The calculated GR contribution of HIO₃ and H₂SO₄ to sub-3 nm particles (ratio 1.5–3) are listed in Table S8, where the statistical ratios of acid contributions for each NPF event are listed as well. The computations of Eqs. (9) and (10) are subject to acid concentrations and hence the average acid concentrations for individual NPF events dominate the statistics of the GR ratio. At the SORPES station from June to November 2019, the contribution of HIO₃ to sub-3 nm particle growth accounts for 6.1% (median) and 6.7% (mean) of H₂SO₄.

As listed in Table S9, estimated particle survival probability of particles growing from 1.5 to 3 nm considering H₂SO₄ as the governing contributor (SP_{1.5–3}(SA)) is significantly enhanced when counting the contribution from HIO₃

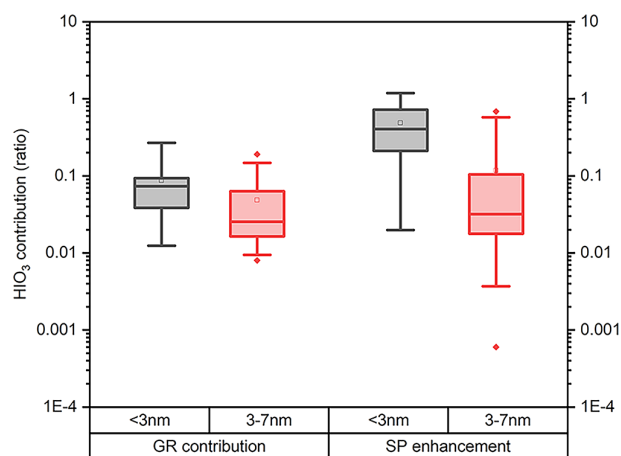


Figure 7. The contributions in ratio of HIO₃ to growth rate (a) and survival probability enhancement (b) of particles within sub-3 and 3–7 nm in NPF events in the Beijing site utilizing the mode fitting method.

(SP_{1.5–3}(SA + IA)). The enhancement of SP with IA being an additional GR contributor varies from 3 % to more than 100 % in favorable cases, with a median enhancement of 54.3 %. For sub-3 nm particles, the survival probability is twice as higher (enhancement factors exceeding 100 %) considering HIO₃ as an additional GR contributor on 3 July and 26 October. As depicted in Fig. S11c, SP enhancements in percentage are generally an order of magnitude higher than the GR contribution in percentage, and HIO₃ can result in as high as 2-fold enhancement of SP in sub-3 nm particle growth.

The statistical results at both sites suggest that for polluted environments with higher CoagS, GR enhancement is especially important for the survival of small particles. In Beijing, HIO₃ contributes 7.4 % (median) to sub-3 nm particle growth and 2.6 % (median) to 3–7 nm particle growth in all NPF events from May to September. Despite the limited GR contribution, it could lead to 40.5 % enhancement of SP_{<3}, whereas there is only a negligible increase of 3.2 % (median) for SP_{3–7} estimated using the MOD method. In exceptional cases, we found that HIO₃ could enhance particle SP by more than 2-fold in 22.2 % of cases. The median value of GR contribution of HIO₃ accounts for 6.1 % of H₂SO₄ and the median enhancement of 1.5–3 nm particles survival probability reaches 47.6 % when considering HIO₃ as an additional GR contributor at the SORPES station in summer 2019. In favorable cases, the gaseous HIO₃ can contribute to more than 14.0 % of particle growth, leading to the survival probability of fresh particles being enhanced by a factor of 2. The role of the other iodine oxoacid, HIO₂, in particle growth remains unclear due to the absence of contribution equation like Eq. (10) for HIO₃. The estimated contribution of HIO₂ derived from the same equation should be significantly smaller compared with that of HIO₃ even if the arrival

rate of HIO₂ also reaches the kinetic limit, as measured HIO₂ concentrations at both sites are much lower than HIO₃.

In summary, our findings show that HIO₃ is an important contributor to sub-3 nm particle survival in these two Chinese cities and similar environments elsewhere in warm seasons. However, for particles of 3–7 nm, the contribution of HIO₃ to particle GR and SP is negligible.

4 Conclusion

In this study, we show 3 years of measurements of iodine oxoacids (HIO_x) in Beijing and a 1-year observation in Nanjing. Unlike H₂SO₄, HIO₃ has a more prominent seasonal variation at both sites with the highest concentrations in summer and lowest concentrations in winter. The diurnal pattern of HIO_x indicates that HIO₃ formation is influenced by photochemical activities and O₃ concentrations, which may together influence the emission of iodine species and the further oxidation chemistry. In Beijing, back trajectory analysis suggests that marine iodine sources are important for the HIO_x production and less HIO_x is observed if the air masses originate from the North. The lowest concentrations of HIO_x in winter and its weak correlation with PM_{2.5} implies that anthropogenic activities are likely not the important sources of HIO_x.

We find that the median contribution of iodic acid, HIO₃, to GR_{sub-3} is less than 10 % in Beijing and in Nanjing from May to September. However, HIO₃ can significantly enhance particle survival probability, occasionally by 2-fold, for 1.5–3 nm particles at both sites. This means that although H₂SO₄ is considered to be the main driver of sub-3 nm growth in polluted urban areas, additional sources, such as HIO₃, need to be considered. As the growth rate of HIO₃ is measured to be identical to that of H₂SO₄ on a per-molecule basis (He et al., 2021b), we propose that HIO₃ and H₂SO₄ can be summed up when estimating the sub-3 nm particle growth rates. Besides the enhancement to particle growth, recent theoretical studies have indicated that dimethylamine could potentially accelerate pure HIO₃ nucleation (Ning et al., 2022). However, experimental confirmation is needed to confirm such prediction, and our long-term observation can therefore provide a basis for guiding experimental works to use ambient relevant levels of acid concentrations.

Data availability. Measurement data at the AHL/BUCT and SORPES station, including acid concentration data, trace gas and aerosol data, and meteorological data, are available upon request from the corresponding authors before the relevant databases are open to the public.

Supplement. The supplement related to this article is available online at: <https://doi.org/10.5194/acp-24-1873-2024-supplement>.

Author contributions. WN and XCH designed the research. YZ, CD, YG, YirL, CH, TL, and ZW conducted the measurements at the AHL/BUCT station. DL, YulL, CL, LC, YuaL, LW, and XC conducted the measurements at the SORPES station. YZ, DL, XCH, WN, CD, RC, YulL, YG, TP, FB, XQ, PP, YonL, CY, JJ, AD, and MK analyzed the data and interpreted the results. YZ, DL, XCH, and WN prepared the manuscript with contributions from all co-authors.

Competing interests. At least one of the (co-)authors is a member of the editorial board of *Atmospheric Chemistry and Physics*. The peer-review process was guided by an independent editor, and the authors also have no other competing interests to declare.

Disclaimer. Publisher's note: Copernicus Publications remains neutral with regard to jurisdictional claims made in the text, published maps, institutional affiliations, or any other geographical representation in this paper. While Copernicus Publications makes every effort to include appropriate place names, the final responsibility lies with the authors.

Acknowledgements. We thank our colleagues and students at the AHL/BUCT station and the SORPES station for their contributions to the maintenance of the measurements.

Financial support. This research has been supported by the National Natural Science Foundation of China (grant nos. 92044301, 42220104006, 42075101 and 41975154), the Academy of Finland, Luonnontieteiden ja Tekniikan Tutkimuksen Toimikunta (grant nos. 337549, 302958, 325656, 316114, 314798, 325647, 341349 and 349659), the European Research Council, H2020 European Research Council (grant no. 742206), the Jiangsu Provincial Collaborative Innovation Center of Climate Change, the Fundamental Research Funds for the Central Universities, and Samsung PM_{2.5} SRP.

Open-access funding was provided by the Helsinki University Library.

Review statement. This paper was edited by Steven Brown and reviewed by two anonymous referees.

References

Almeida, J., Schobesberger, S., Kürten, A., Ortega, I. K., Kupiainen-Määttä, O., Praplan, A. P., Adamov, A., Amorim, A., Bianchi, F., Breitenlechner, M., David, A., Dommen, J., Donahue, N. M., Downard, A., Dunne, E., Duplissy, J., Ehrhart, S., Flagan, R. C., Franchin, A., Guida, R., Hakala, J., Hansel, A., Heinritzi, M., Henschel, H., Jokinen, T., Junninen, H., Kajos, M., Kangasluoma, J., Keskinen, H., Kupc, A., Kurtén, T., Kvashin, A. N., Laaksonen, A., Lehtipalo, K., Leiminger, M., Leppä, J., Loukonen, V., Makhmutov, V., Mathot, S., McGrath, M. J.,

Nieminen, T., Olenius, T., Onnela, A., Petäjä, T., Riccobono, F., Riipinen, I., Rissanen, M., Rondo, L., Ruuskanen, T., Santos, F. D., Sarnela, N., Schallhart, S., Schnitzhofer, R., Seinfeld, J. H., Simon, M., Sipilä, M., Stozhkov, Y., Stratmann, F., Tomé, A., Tröstl, J., Tsigkogeorgas, G., Vaattovaara, P., Viisanen, Y., Virtanen, A., Vrtala, A., Wagner, P. E., Weingartner, E., Wex, H., Williamson, C., Wimmer, D., Ye, P., Yli-Juuti, T., Carslaw, K. S., Kulmala, M., Curtius, J., Baltensperger, U., Worsnop, D. R., Vehkamäki, H., and Kirkby, J.: Molecular understanding of sulphuric acid–amine particle nucleation in the atmosphere. *Nature*, 502, 359–363, <https://doi.org/10.1038/nature12663>, 2013.

Andreae, M. O., Atlas, E., Harris, G. W., Helas, G., de Kock, A., Koppmann, R., Maenhaut, W., Manø, S., Pollock, W. H., Rudolph, J., Scharffe, D., Schebeske, G., and Welling, M.: Methyl halide emissions from savanna fires in southern Africa. *J. Geophys. Res.-Atmos.*, 101, 23603–23613, <https://doi.org/10.1029/95jd01733>, 1996.

Baccarini, A., Karlsson, L., Dommen, J., Duplessis, P., Vullers, J., Brooks, I. M., Saiz-Lopez, A., Salter, M., Tjernstrom, M., Baltensperger, U., Zieger, P., and Schmale, J.: Frequent new particle formation over the high Arctic pack ice by enhanced iodine emissions. *Nat. Commun.*, 11, 4924, <https://doi.org/10.1038/s41467-020-18551-0>, 2020.

Beck, L. J., Sarnela, N., Junninen, H., Hoppe, C. J. M., Garmash, O., Bianchi, F., Riva, M., Rose, C., Peräkylä, O., Wimmer, D., Kausiala, O., Jokinen, T., Ahonen, L., Mikkilä, J., Hakala, J., He, X. C., Kontkanen, J., Wolf, K. K. E., Cappelletti, D., Mazzola, M., Traversi, R., Petroselli, C., Viola, A. P., Vitale, V., Lange, R., Massling, A., Nøjgaard, J. K., Krejci, R., Karlsson, L., Zieger, P., Jang, S., Lee, K., Vakkari, V., Lampilahti, J., Thakur, R. C., Leino, K., Kangasluoma, J., Duplissy, E. M., Siivola, E., Marbouti, M., Tham, Y. J., Saiz-Lopez, A., Petäjä, T., Ehn, M., Worsnop, D. R., Skov, H., Kulmala, M., Kerminen, V. M., and Sipilä, M.: Differing Mechanisms of New Particle Formation at Two Arctic Sites. *Geophys. Res. Lett.*, 48, e2020GL091334, <https://doi.org/10.1029/2020gl091334>, 2021.

Bousiotis, D., Brean, J., Pope, F. D., Dall'Osto, M., Querol, X., Alastuey, A., Perez, N., Petäjä, T., Massling, A., Nøjgaard, J. K., Nordstrøm, C., Kouvarakis, G., Vratolis, S., Eleftheriadis, K., Niemi, J. V., Portin, H., Wiedensohler, A., Weinhold, K., Merkel, M., Tuch, T., and Harrison, R. M.: The effect of meteorological conditions and atmospheric composition in the occurrence and development of new particle formation (NPF) events in Europe. *Atmos. Chem. Phys.*, 21, 3345–3370, <https://doi.org/10.5194/acp-21-3345-2021>, 2021.

Cai, M., Liang, B., Sun, Q., Liu, L., Yuan, B., Shao, M., Huang, S., Peng, Y., Wang, Z., Tan, H., Li, F., Xu, H., Chen, D., and Zhao, J.: The important roles of surface tension and growth rate in the contribution of new particle formation (NPF) to cloud condensation nuclei (CCN) number concentration: evidence from field measurements in southern China. *Atmos. Chem. Phys.*, 21, 8575–8592, <https://doi.org/10.5194/acp-21-8575-2021>, 2021.

Cai, R., Chen, D.-R., Hao, J., and Jiang, J.: A miniature cylindrical differential mobility analyzer for sub-3 nm particle sizing. *J. Aerosol Sci.*, 106, 111–119, <https://doi.org/10.1016/j.jaerosci.2017.01.004>, 2017a.

Cai, R., Yang, D., Fu, Y., Wang, X., Li, X., Ma, Y., Hao, J., Zheng, J., and Jiang, J.: Aerosol surface area concentration: a governing factor in new particle formation in Beijing. *Atmos. Chem.*

- Phys., 17, 12327–12340, <https://doi.org/10.5194/acp-17-12327-2017>, 2017b.
- Cai, R., Yan, C., Worsnop, D. R., Bianchi, F., Kerminen, V.-M., Liu, Y., Wang, L., Zheng, J., Kulmala, M., and Jiang, J.: An indicator for sulfuric acid–amine nucleation in atmospheric environments, *Aerosol Sci. Tech.*, 55, 1059–1069, <https://doi.org/10.1080/02786826.2021.1922598>, 2021a.
- Cai, R., Li, C., He, X.-C., Deng, C., Lu, Y., Yin, R., Yan, C., Wang, L., Jiang, J., Kulmala, M., and Kangasluoma, J.: Impacts of coagulation on the appearance time method for new particle growth rate evaluation and their corrections, *Atmos. Chem. Phys.*, 21, 2287–2304, <https://doi.org/10.5194/acp-21-2287-2021>, 2021b.
- Cai, R., Yan, C., Yang, D., Yin, R., Lu, Y., Deng, C., Fu, Y., Ruan, J., Li, X., Kontkanen, J., Zhang, Q., Kangasluoma, J., Ma, Y., Hao, J., Worsnop, D. R., Bianchi, F., Paasonen, P., Kerminen, V.-M., Liu, Y., Wang, L., Zheng, J., Kulmala, M., and Jiang, J.: Sulfuric acid–amine nucleation in urban Beijing, *Atmos. Chem. Phys.*, 21, 2457–2468, <https://doi.org/10.5194/acp-21-2457-2021>, 2021c.
- Cai, R., Häkkinen, E., Yan, C., Jiang, J., Kulmala, M., and Kangasluoma, J.: The effectiveness of the coagulation sink of 3–10 nm atmospheric particles, *Atmos. Chem. Phys.*, 22, 11529–11541, <https://doi.org/10.5194/acp-22-11529-2022>, 2022a.
- Cai, R., Yin, R., Yan, C., Yang, D., Deng, C., Dada, L., Kangasluoma, J., Kontkanen, J., Halonen, R., Ma, Y., Zhang, X., Paasonen, P., Petäjä, T., Kerminen, V. M., Liu, Y., Bianchi, F., Zheng, J., Wang, L., Hao, J., Smith, J. N., Donahue, N. M., Kulmala, M., Worsnop, D. R., and Jiang, J.: The missing base molecules in atmospheric acid-base nucleation, *Natl. Sci. Rev.*, 9, nwac137, <https://doi.org/10.1093/nsr/nwac137>, 2022b.
- Carpenter, L. J., MacDonald, S. M., Shaw, M. D., Kumar, R., Saunders, R. W., Parthipan, R., Wilson, J., and Plane, J. M. C.: Atmospheric iodine levels influenced by sea surface emissions of inorganic iodine, *Nat. Geosci.*, 6, 108–111, <https://doi.org/10.1038/ngeo1687>, 2013.
- Carpenter, L. J., Chance, R. J., Sherwen, T., Adams, T. J., Ball, S. M., Evans, M. J., Hepach, H., Hollis, L. D. J., Hughes, C., Jickells, T. D., Mahajan, A., Stevens, D. P., Tinel, L., and Wadley, M. R.: Marine iodine emissions in a changing world, *P. Roy. Soc. A-Math. Phys.*, 477, 2247, <https://doi.org/10.1098/rspa.2020.0824>, 2021.
- Chen, R., Hu, B., Liu, Y., Xu, J., Yang, G., Xu, D., and Chen, C.: Beyond PM_{2.5}: The role of ultrafine particles on adverse health effects of air pollution, *BBA-Gen. Subjects*, 1860, 2844–2855, <https://doi.org/10.1016/j.bbagen.2016.03.019>, 2016.
- Chen, Y., Liu, S., Yang, G., and He, Z.: Influence Factors on Photochemical Production of Methyl Iodide in Seawater, *J. Ocean U. China*, 19, 1353–1361, <https://doi.org/10.1007/s11802-020-4463-8>, 2020.
- Chu, B., Kerminen, V.-M., Bianchi, F., Yan, C., Petäjä, T., and Kulmala, M.: Atmospheric new particle formation in China, *Atmos. Chem. Phys.*, 19, 115–138, <https://doi.org/10.5194/acp-19-115-2019>, 2019.
- Dada, L., Lehtipalo, K., Kontkanen, J., Nieminen, T., Baalbaki, R., Ahonen, L., Duplissy, J., Yan, C., Chu, B., Petäjä, T., Lehtinen, K., Kerminen, V.-M., Kulmala, M., and Kangasluoma, J.: Formation and growth of sub-3-nm aerosol particles in experimental chambers, *Nat. Protoc.*, 15, 1013–1040, <https://doi.org/10.1038/s41596-019-0274-z>, 2020.
- Deng, C., Cai, R., Yan, C., Zheng, J., and Jiang, J.: Formation and growth of sub-3 nm particles in megacities: impact of background aerosols, *Faraday Discuss.*, 226, 348–363, <https://doi.org/10.1039/d0fd00083c>, 2020a.
- Deng, C., Fu, Y., Dada, L., Yan, C., Cai, R., Yang, D., Zhou, Y., Yin, R., Lu, Y., Li, X., Qiao, X., Fan, X., Nie, W., Kontkanen, J., Kangasluoma, J., Chu, B., Ding, A., Kerminen, V. M., Paasonen, P., Worsnop, D. R., Bianchi, F., Liu, Y., Zheng, J., Wang, L., Kulmala, M., and Jiang, J.: Seasonal Characteristics of New Particle Formation and Growth in Urban Beijing, *Environ. Sci. Technol.*, 54, 8547–8557, <https://doi.org/10.1021/acs.est.0c00808>, 2020b.
- Dimmer, C. H., Simmonds, P. G., Nickless, G., and Bassford, M. R. J. A. E.: Biogenic fluxes of halomethanes from Irish peatland ecosystems, *Atmos. Environ.*, 35, 321–330, [https://doi.org/10.1016/S1352-2310\(00\)00151-5](https://doi.org/10.1016/S1352-2310(00)00151-5), 2001.
- Ding, A., Nie, W., Huang, X., Chi, X., Sun, J., Kerminen, V.-M., Xu, Z., Guo, W., Petäjä, T., Yang, X., Kulmala, M., and Fu, C.: Long-term observation of air pollution-weather/climate interactions at the SORPES station: a review and outlook, *Front. Env. Sci. Eng.*, 10, 15, <https://doi.org/10.1007/s11783-016-0877-3>, 2016.
- Ding, A., Huang, X., Nie, W., Chi, X., Xu, Z., Zheng, L., Xu, Z., Xie, Y., Qi, X., Shen, Y., Sun, P., Wang, J., Wang, L., Sun, J., Yang, X.-Q., Qin, W., Zhang, X., Cheng, W., Liu, W., Pan, L., and Fu, C.: Significant reduction of PM_{2.5} in eastern China due to regional-scale emission control: evidence from SORPES in 2011–2018, *Atmos. Chem. Phys.*, 19, 11791–11801, <https://doi.org/10.5194/acp-19-11791-2019>, 2019.
- Downward, G. S., van Nunen, E., Kerckhoffs, J., Vineis, P., Brunekreef, B., Boer, J. M. A., Messier, K. P., Roy, A., Verschuren, W. M. M., van der Schouw, Y. T., Sluijs, I., Gulliver, J., Hoek, G., and Vermeulen, R.: Long-Term Exposure to Ultrafine Particles and Incidence of Cardiovascular and Cerebrovascular Disease in a Prospective Study of a Dutch Cohort, *Environ. Health Persp.*, 126, 127007, <https://doi.org/10.1289/EHP3047>, 2018.
- Drougas, E. and Kosmas, A. M.: Computational Studies of (HIO₃) Isomers and the HO₂ + IO Reaction Pathways, *J. Phys. Chem. A*, 109, 3887–3892, <https://doi.org/10.1021/jp044197j>, 2005.
- Ehn, M., Thornton, J. A., Kleist, E., Sipilä, M., Junninen, H., Pullinen, I., Springer, M., Rubach, F., Tillmann, R., Lee, B., Lopez-Hilfiker, F., Andres, S., Acir, I.-H., Rissanen, M., Jokinen, T., Schobesberger, S., Kangasluoma, J., Kontkanen, J., Nieminen, T., Kurtén, T., Nielsen, L. B., Jørgensen, S., Kjaergaard, H. G., Canagaratna, M., Maso, M. D., Berndt, T., Petäjä, T., Wahner, A., Kerminen, V.-M., Kulmala, M., Worsnop, D. R., Wildt, J., and Mentel, T. F.: A large source of low-volatility secondary organic aerosol, *Nature*, 506, 476–479, <https://doi.org/10.1038/nature13032>, 2014.
- Finkenzeller, H., Iyer, S., He, X.-C., Simon, M., Koenig, T. K., Lee, C. F., Valiev, R., Hofbauer, V., Amorim, A., Baalbaki, R., Baccharini, A., Beck, L., Bell, D. M., Caudillo, L., Chen, D., Chiu, R., Chu, B., Dada, L., Duplissy, J., Heinritzi, M., Kempainen, D., Kim, C., Krechmer, J., Kürten, A., Kvashnin, A., Lamkaddam, H., Lee, C. P., Lehtipalo, K., Li, Z., Makhmutov, V., Manninen, H. E., Marie, G., Marten, R., Mauldin, R. L., Mentler, B., Müller, T., Petäjä, T., Philippov, M., Ranjithkumar, A., Rörup, B., Shen, J., Stolzenburg, D., Tauber, C., Tham, Y. J., Tomé, A., Vazquez-Pufeu, M., Wagner, A. C., Wang, D. S., Wang, M., Wang, Y., Weber, S. K., Nie, W., Wu, Y., Xiao, M., Ye, Q., Zauner-

- Wieczorek, M., Hansel, A., Baltensperger, U., Brioude, J., Curtius, J., Donahue, N. M., Haddad, I. E., Flagan, R. C., Kulmala, M., Kirkby, J., Sipilä, M., Worsnop, D. R., Kurten, T., Rissanen, M., and Volkamer, R.: The gas-phase formation mechanism of iodic acid as an atmospheric aerosol source, *Nat. Chem.*, 15, 129–135, <https://doi.org/10.1038/s41557-022-01067-z>, 2023.
- Fuchs, N. A. and Sutugin, A. G.: High-Dispersed Aerosols, in: Topics in Current Aerosol Research, edited by: Hidy, G. M. and Brock, J. R., Pergamon, p. 1, <https://doi.org/10.1016/B978-0-08-016674-2.50006-6>, 1971.
- Gomez Martin, J. C., Lewis, T. R., Blitz, M. A., Plane, J. M. C., Kumar, M., Francisco, J. S., and Saiz-Lopez, A.: A gas-to-particle conversion mechanism helps to explain atmospheric particle formation through clustering of iodine oxides, *Nat. Commun.*, 11, 4521, <https://doi.org/10.1038/s41467-020-18252-8>, 2020.
- Guo, Y., Yan, C., Li, C., Ma, W., Feng, Z., Zhou, Y., Lin, Z., Dada, L., Stolzenburg, D., Yin, R., Kontkanen, J., Daellenbach, K. R., Kangasluoma, J., Yao, L., Chu, B., Wang, Y., Cai, R., Bianchi, F., Liu, Y., and Kulmala, M.: Formation of nighttime sulfuric acid from the ozonolysis of alkenes in Beijing, *Atmos. Chem. Phys.*, 21, 5499–5511, <https://doi.org/10.5194/acp-21-5499-2021>, 2021.
- He, X.-C.: From the measurement of halogenated species to iodine particle formation, MS thesis, University of Helsinki, Helsinki, <https://helda.helsinki.fi/handle/10138/229173> (last access: 9 February 2024), 2017.
- He, X.-C., Iyer, S., Sipilä, M., Ylisirniö, A., Peltola, M., Kontkanen, J., Baalbaki, R., Simon, M., Kürten, A., Tham, Y. J., Pesonen, J., Ahonen, L. R., Amanatidis, S., Amorim, A., Baccarini, A., Beck, L., Bianchi, F., Brilke, S., Chen, D., Chiu, R., Curtius, J., Dada, L., Dias, A., Dommen, J., Donahue, N. M., Duplissy, J., El Haddad, I., Finkenzeller, H., Fischer, L., Heinritzi, M., Hofbauer, V., Kangasluoma, J., Kim, C., Koenig, T. K., Kubečka, J., Kvashnin, A., Lamkaddam, H., Lee, C. P., Leiminger, M., Li, Z., Makhmutov, V., Xiao, M., Marten, R., Nie, W., Onnela, A., Partoll, E., Petäjä, T., Salo, V.-T., Schuchmann, S., Steiner, G., Stolzenburg, D., Stozhkov, Y., Tauber, C., Tomé, A., Väisänen, O., Vazquez-Pufleau, M., Volkamer, R., Wagner, A. C., Wang, M., Wang, Y., Wimmer, D., Winkler, P. M., Worsnop, D. R., Wu, Y., Yan, C., Ye, Q., Lehtinen, K., Nieminen, T., Manninen, H. E., Rissanen, M., Schobesberger, S., Lehtipalo, K., Baltensperger, U., Hansel, A., Kerminen, V.-M., Flagan, R. C., Kirkby, J., Kurtén, T., and Kulmala, M.: Determination of the collision rate coefficient between charged iodic acid clusters and iodic acid using the appearance time method, *Aerosol Sci. Tech.*, 55, 231–242, <https://doi.org/10.1080/02786826.2020.1839013>, 2021a.
- He, X.-C., Tham, Y. J., Dada, L., Wang, M., Finkenzeller, H., Stolzenburg, D., Iyer, S., Simon, M., Kürten, A., Shen, J., Rörup, B., Rissanen, M., Schobesberger, S., Baalbaki, R., Wang, D. S., Koenig, T. K., Jokinen, T., Sarnela, N., Beck, L. J., Almeida, J., Amanatidis, S., Amorim, A., Ataei, F., Baccarini, A., Bertozzi, B., Bianchi, F., Brilke, S., Caudillo, L., Chen, D., Chiu, R., Chu, B., Dias, A., Ding, A., Dommen, J., Duplissy, J., El Haddad, I., Gonzalez Carracedo, L., Granzin, M., Hansel, A., Heinritzi, M., Hofbauer, V., Junninen, H., Kangasluoma, J., Kempainen, D., Kim, C., Kong, W., Krechmer, J. E., Kvashin, A., Laitinen, T., Lamkaddam, H., Lee, C. P., Lehtipalo, K., Leiminger, M., Li, Z., Makhmutov, V., Manninen, H. E., Marie, G., Marten, R., Mathot, S., Mauldin, R. L., Mentler, B., Möhler, O., Müller, T., Nie, W., Onnela, A., Petäjä, T., Pfeifer, J., Philippov, M., Ranjithkumar, A., Saiz-Lopez, A., Salma, I., Scholz, W., Schuchmann, S., Schulze, B., Steiner, G., Stozhkov, Y., Tauber, C., Tomé, A., Thakur, R. C., Väisänen, O., Vazquez-Pufleau, M., Wagner, A. C., Wang, Y., Weber, S. K., Winkler, P. M., Wu, Y., Xiao, M., Yan, C., Ye, Q., Ylisirniö, A., Zauner-Wieczorek, M., Zha, Q., Zhou, P., Flagan, R. C., Curtius, J., Baltensperger, U., Kulmala, M., Kerminen, V.-M., Kurtén, T., Donahue, N. M., Volkamer, R., Kirkby, J., Worsnop, D. R., and Sipilä, M.: Role of iodine oxoacids in atmospheric aerosol nucleation, *Science*, 371, 589–595, <https://doi.org/10.1126/science.abe0298>, 2021b.
- He, X.-C., Shen, J., Iyer, S., Juuti, P., Zhang, J., Koirala, M., Kytökari, M. M., Worsnop, D. R., Rissanen, M., Kulmala, M., Maier, N. M., Mikkilä, J., Sipilä, M., and Kangasluoma, J.: Characterisation of gaseous iodine species detection using the multi-scheme chemical ionisation inlet 2 with bromide and nitrate chemical ionisation methods, *Atmos. Meas. Tech.*, 16, 4461–4487, <https://doi.org/10.5194/amt-16-4461-2023>, 2023.
- Hoffmann, T., O'Dowd, C. D., and Seinfeld, J. H.: Iodine oxide homogeneous nucleation: An explanation for coastal new particle production, *Geophys. Res. Lett.*, 28, 1949–1952, <https://doi.org/10.1029/2000gl012399>, 2001.
- Jiang, J., Chen, M., Kuang, C., Attoui, M., and McMurry, P. H.: Electrical Mobility Spectrometer Using a Diethylene Glycol Condensation Particle Counter for Measurement of Aerosol Size Distributions Down to 1 nm, *Aerosol Sci. Tech.*, 45, 510–521, <https://doi.org/10.1080/02786826.2010.547538>, 2011.
- Jiang, S., Zhang, F., Ren, J., Chen, L., Yan, X., Liu, J., Sun, Y., and Li, Z.: Evaluation of the contribution of new particle formation to cloud droplet number concentration in the urban atmosphere, *Atmos. Chem. Phys.*, 21, 14293–14308, <https://doi.org/10.5194/acp-21-14293-2021>, 2021.
- Jimenez, J. L.: New particle formation from photooxidation of diiodomethane (CH₂I₂), *J. Geophys. Res.*, 108, 4318, <https://doi.org/10.1029/2002jd002452>, 2003.
- Jokinen, T., Sipilä, M., Junninen, H., Ehn, M., Lönn, G., Hakala, J., Petäjä, T., Mauldin III, R. L., Kulmala, M., and Worsnop, D. R.: Atmospheric sulphuric acid and neutral cluster measurements using CI-API-TOF, *Atmos. Chem. Phys.*, 12, 4117–4125, <https://doi.org/10.5194/acp-12-4117-2012>, 2012.
- Jokinen, T., Sipilä, M., Kontkanen, J., Vakkari, V., Tisler, P., Duplissy, E. M., Junninen, H., Kangasluoma, J., Manninen, H. E., Petaja, T., Kulmala, M., Worsnop, D. R., Kirkby, J., Virkkula, A., and Kerminen, V. M.: Ion-induced sulfuric acid-ammonia nucleation drives particle formation in coastal Antarctica, *Sci. Adv.*, 4, <https://doi.org/10.1126/sciadv.aat9744>, 2018.
- Jokinen, T., Lehtipalo, K., Thakur, R. C., Ylivinkka, I., Neitola, K., Sarnela, N., Laitinen, T., Kulmala, M., Petäjä, T., and Sipilä, M.: Measurement report: Long-term measurements of aerosol precursor concentrations in the Finnish subarctic boreal forest, *Atmos. Chem. Phys.*, 22, 2237–2254, <https://doi.org/10.5194/acp-22-2237-2022>, 2022.
- Junninen, H., Ehn, M., Petäjä, T., Luosujärvi, L., Kotiaho, T., Koskiainen, R., Rohner, U., Gonin, M., Fuhrer, K., Kulmala, M., and Worsnop, D. R.: A high-resolution mass spectrometer to measure atmospheric ion composition, *Atmos. Meas. Tech.*, 3, 1039–1053, <https://doi.org/10.5194/amt-3-1039-2010>, 2010.
- Kalkavouras, P., Bossioli, E., Bezantakos, S., Bougiatioti, A., Kalivitis, N., Stavroulas, I., Kouvarakis, G., Protonotariou, A.

- P., Dandou, A., Biskos, G., Mihalopoulos, N., Nenes, A., and Tombrou, M.: New particle formation in the southern Aegean Sea during the Etesians: importance for CCN production and cloud droplet number, *Atmos. Chem. Phys.*, 17, 175–192, <https://doi.org/10.5194/acp-17-175-2017>, 2017.
- Kalkavouras, P., Bougiatioti, A., Kalivitis, N., Stavroulas, I., Tombrou, M., Nenes, A., and Mihalopoulos, N.: Regional new particle formation as modulators of cloud condensation nuclei and cloud droplet number in the eastern Mediterranean, *Atmos. Chem. Phys.*, 19, 6185–6203, <https://doi.org/10.5194/acp-19-6185-2019>, 2019.
- Kerminen, V.-M., Lihavainen, H., Komppula, M., Viisanen, Y., and Kulmala, M.: Direct observational evidence linking atmospheric aerosol formation and cloud droplet activation, *Geophys. Res. Lett.*, 32, L14803, <https://doi.org/10.1029/2005gl023130>, 2005.
- Kerminen, V.-M., Chen, X., Vakkari, V., Petäjä, T., Kulmala, M., and Bianchi, F.: Atmospheric new particle formation and growth: review of field observations, *Environ. Res. Lett.*, 13, 103003, <https://doi.org/10.1088/1748-9326/aadf3c>, 2018.
- Kirkby, J., Curtius, J., Almeida, J., Dunne, E., Duplissy, J., Ehrhart, S., Franchin, A., Gagné, S., Ickes, L., Kürten, A., Kupc, A., Metzger, A., Riccobono, F., Rondo, L., Schobesberger, S., Tsagko-georgas, G., Wimmer, D., Amorim, A., Bianchi, F., Breitenlechner, M., David, A., Dommen, J., Downard, A., Ehn, M., Flagan, R. C., Haider, S., Hansel, A., Hauser, D., Jud, W., Junninen, H., Kreissl, F., Kvashin, A., Laaksonen, A., Lehtipalo, K., Lima, J., Lovejoy, E. R., Makhmutov, V., Mathot, S., Mikkilä, J., Minginette, P., Mogo, S., Nieminen, T., Onnela, A., Pereira, P., Petäjä, T., Schnitzhofer, R., Seinfeld, J. H., Sipilä, M., Stozhkov, Y., Stratmann, F., Tomé, A., Vanhanen, J., Viisanen, Y., Vrtala, A., Wagner, P. E., Walther, H., Weingartner, E., Wex, H., Winkler, P. M., Carslaw, K. S., Worsnop, D. R., Baltensperger, U., and Kulmala, M.: Role of sulphuric acid, ammonia and galactic cosmic rays in atmospheric aerosol nucleation, *Nature*, 476, 429–433, <https://doi.org/10.1038/nature10343>, 2011.
- Kirkby, J., Duplissy, J., Sengupta, K., Frege, C., Gordon, H., Williamson, C., Heinritzi, M., Simon, M., Yan, C., Almeida, J., Tröstl, J., Nieminen, T., Ortega, I. K., Wagner, R., Adamov, A., Amorim, A., Bernhammer, A.-K., Bianchi, F., Breitenlechner, M., Brilke, S., Chen, X., Craven, J., Dias, A., Ehrhart, S., Flagan, R. C., Franchin, A., Fuchs, C., Guida, R., Hakala, J., Hoyle, C. R., Jokinen, T., Junninen, H., Kangasluoma, J., Kim, J., Krapf, M., Kürten, A., Laaksonen, A., Lehtipalo, K., Makhmutov, V., Mathot, S., Molteni, U., Onnela, A., Peräkylä, O., Piel, F., Petäjä, T., Praplan, A. P., Pringle, K., Rap, A., Richards, N. A. D., Riipinen, I., Rissanen, M. P., Rondo, L., Sarnela, N., Schobesberger, S., Scott, C. E., Seinfeld, J. H., Sipilä, M., Steiner, G., Stozhkov, Y., Stratmann, F., Tomé, A., Virtanen, A., Vogel, A. L., Wagner, A. C., Wagner, P. E., Weingartner, E., Wimmer, D., Winkler, P. M., Ye, P., Zhang, X., Hansel, A., Dommen, J., Donahue, N. M., Worsnop, D. R., Baltensperger, U., Kulmala, M., Carslaw, K. S., and Curtius, J.: Ion-induced nucleation of pure biogenic particles, *Nature*, 533, 521–526, <https://doi.org/10.1038/nature17953>, 2016.
- Kuang, C., Riipinen, I., Sihto, S.-L., Kulmala, M., McCormick, A. V., and McMurry, P. H.: An improved criterion for new particle formation in diverse atmospheric environments, *Atmos. Chem. Phys.*, 10, 8469–8480, <https://doi.org/10.5194/acp-10-8469-2010>, 2010.
- Kuang, C., Chen, M., Zhao, J., Smith, J., McMurry, P. H., and Wang, J.: Size and time-resolved growth rate measurements of 1 to 5 nm freshly formed atmospheric nuclei, *Atmos. Chem. Phys.*, 12, 3573–3589, <https://doi.org/10.5194/acp-12-3573-2012>, 2012.
- Kulmala, M., Maso, M. D., Mäkelä, J., Pirjola, L., Väkevä, M., Aalto, P., Miikkulainen, P., Hämeri, K., and O'Dowd, C. J. T. B.: On the formation, growth and composition of nucleation mode particles, *Tellus B*, 53, 479–490, 2001.
- Kulmala, M., Kerminen, V. M., Anttila, T., Laaksonen, A., and O'Dowd, C. D.: Organic aerosol formation via sulphate cluster activation, *J. Geophys. Res.-Atmos.*, 109, D04205, <https://doi.org/10.1029/2003jd003961>, 2004a.
- Kulmala, M., Vehkamäki, H., Petäjä, T., Dal Maso, M., Lauri, A., Kerminen, V. M., Birmili, W., and McMurry, P. H.: Formation and growth rates of ultrafine atmospheric particles: a review of observations, *J. Aerosol Sci.*, 35, 143–176, <https://doi.org/10.1016/j.jaerosci.2003.10.003>, 2004b.
- Kulmala, M., Petäjä, T., Nieminen, T., Sipilä, M., Manninen, H. E., Lehtipalo, K., Dal Maso, M., Aalto, P. P., Junninen, H., Paasonen, P., Riipinen, I., Lehtinen, K. E. J., Laaksonen, A., and Kerminen, V.-M.: Measurement of the nucleation of atmospheric aerosol particles, *Nat. Protoc.*, 7, 1651–1667, <https://doi.org/10.1038/nprot.2012.091>, 2012.
- Kulmala, M., Kerminen, V. M., Petaja, T., Ding, A. J., and Wang, L.: Atmospheric gas-to-particle conversion: why NPF events are observed in megacities?, *Faraday Discuss.*, 200, 271–288, <https://doi.org/10.1039/c6fd00257a>, 2017.
- Kulmala, M., Dada, L., Daellenbach, K. R., Yan, C., Stolzenburg, D., Kontkanen, J., Ezhova, E., Hakala, S., Tuovinen, S., Kokkonen, T. V., Kurppa, M., Cai, R., Zhou, Y., Yin, R., Baalbaki, R., Chan, T., Chu, B., Deng, C., Fu, Y., Ge, M., He, H., Heikkinen, L., Junninen, H., Liu, Y., Lu, Y., Nie, W., Rusanen, A., Vakkari, V., Wang, Y., Yang, G., Yao, L., Zheng, J., Kujansuu, J., Kangasluoma, J., Petaja, T., Paasonen, P., Jarvi, L., Worsnop, D., Ding, A., Liu, Y., Wang, L., Jiang, J., Bianchi, F., and Kerminen, V. M.: Is reducing new particle formation a plausible solution to mitigate particulate air pollution in Beijing and other Chinese megacities?, *Faraday Discuss.*, 226, 334–347, <https://doi.org/10.1039/d0fd00078g>, 2021.
- Kulmala, M., Cai, R., Stolzenburg, D., Zhou, Y., Dada, L., Guo, Y., Yan, C., Petäjä, T., Jiang, J., and Kerminen, V. M.: The contribution of new particle formation and subsequent growth to haze formation, *Environ. Sci. Atmos.*, 2, 352–361, <https://doi.org/10.1039/d1ea00096a>, 2022.
- Kürten, A., Rondo, L., Ehrhart, S., and Curtius, J.: Calibration of a Chemical Ionization Mass Spectrometer for the Measurement of Gaseous Sulphuric Acid, *J. Phys. Chem. A*, 116, 6375–6386, <https://doi.org/10.1021/jp212123n>, 2012.
- Kürten, A., Bergen, A., Heinritzi, M., Leiminger, M., Lorenz, V., Piel, F., Simon, M., Sitals, R., Wagner, A. C., and Curtius, J.: Observation of new particle formation and measurement of sulfuric acid, ammonia, amines and highly oxidized organic molecules at a rural site in central Germany, *Atmos. Chem. Phys.*, 16, 12793–12813, <https://doi.org/10.5194/acp-16-12793-2016>, 2016.
- Laakso, L., Petäjä, T., Lehtinen, K. E. J., Kulmala, M., Paatero, J., Hörrak, U., Tammet, H., and Joutsensaari, J.: Ion production rate in a boreal forest based on ion, particle and radiation measurements, *Atmos. Chem. Phys.*, 4, 1933–1943, <https://doi.org/10.5194/acp-4-1933-2004>, 2004.

- Lehtinen, K. E. J., Korhonen, H., Dal Maso, M., and Kulmala, M.: On the concept of condensation sink diameter, *Boreal Environ. Res.*, 8, 405–411, 2003.
- Lehtinen, K. E. J., Dal Maso, M., Kulmala, M., and Kerminen, V.-M.: Estimating nucleation rates from apparent particle formation rates and vice versa: Revised formulation of the Kerminen–Kulmala equation, *J. Aerosol Sci.*, 38, 988–994, <https://doi.org/10.1016/j.jaerosci.2007.06.009>, 2007.
- Lehtipalo, K., Leppä, J., Kontkanen, J., Kangasluoma, J., Franchin, A., Wimmer, D., Schobesberger, S., Junninen, H., Petäjä, T., Sipilä, M., Mikkilä, J., Vanhanen, J., Worsnop, D. R., and Kulmala, M.: Methods for determining particle size distribution and growth rates between 1 and 3 nm using the Particle Size Magnifier, *Boreal Environ. Res.*, 19, 215–236, 2014.
- Lehtipalo, K., Yan, C., Dada, L., Bianchi, F., Xiao, M., Wagner, R., Stolzenburg, D., Ahonen, L. R., Amorim, A., Baccarini, A., Bauer, P. S., Baumgartner, B., Bergen, A., Bernhammer, A. K., Breitenlechner, M., Brilke, S., Buchholz, A., Mazon, S. B., Chen, D., Chen, X., Dias, A., Dommen, J., Draper, D. C., Duplissy, J., Ehn, M., Finkenzeller, H., Fischer, L., Frege, C., Fuchs, C., Garmash, O., Gordon, H., Hakala, J., He, X., Heikkinen, L., Heinritzi, M., Helm, J. C., Hofbauer, V., Hoyle, C. R., Jokinen, T., Kangasluoma, J., Kerminen, V. M., Kim, C., Kirkby, J., Kontkanen, J., Kürten, A., Lawler, M. J., Mai, H., Mathot, S., Mauldin, R. L., 3rd, Molteni, U., Nichman, L., Nie, W., Nieminen, T., Ojdanic, A., Onnela, A., Passananti, M., Petäjä, T., Piel, F., Pospisilova, V., Quéléver, L. L. J., Rissanen, M. P., Rose, C., Sarnela, N., Schallhart, S., Schuchmann, S., Sengupta, K., Simon, M., Sipilä, M., Tauber, C., Tomé, A., Tröstl, J., Väisänen, O., Vogel, A. L., Volkamer, R., Wagner, A. C., Wang, M., Weitz, L., Wimmer, D., Ye, P., Ylisirniö, A., Zha, Q., Carslaw, K. S., Curtius, J., Donahue, N. M., Flagan, R. C., Hansel, A., Riipinen, I., Virtanen, A., Winkler, P. M., Baltensperger, U., Kulmala, M., and Worsnop, D. R.: Multicomponent new particle formation from sulfuric acid, ammonia, and biogenic vapors, *Sci. Adv.*, 4, eaau5363, <https://doi.org/10.1126/sciadv.aau5363>, 2018.
- Li, H., Ning, A., Zhong, J., Zhang, H., Liu, L., Zhang, Y., Zhang, X., Zeng, X. C., and He, H.: Influence of atmospheric conditions on sulfuric acid-dimethylamine-ammonia-based new particle formation, *Chemosphere*, 245, 125554, <https://doi.org/10.1016/j.chemosphere.2019.125554>, 2020.
- Li, Y., Chi, L., Mao, L., Yan, D., Wu, Z., Ma, T., Guo, M., Wang, Q., Ouyang, C., and Cao, A.: Control of Soilborne Pathogens of *Zingiber officinale* by Methyl Iodide and Chloropicrin in China, *Plant Dis.*, 98, 384–388, <https://doi.org/10.1094/PDIS-06-13-0623-RE>, 2014.
- Li, Y., He, Z., Yang, G. P., and Zou, Y.: Spatial distribution and biogeochemical cycling of methyl iodide in the Yellow Sea and the East China Sea during summer, *Environ. Pollut.*, 276, 116749, <https://doi.org/10.1016/j.envpol.2021.116749>, 2021.
- Liu, J., Jiang, J., Zhang, Q., Deng, J., and Hao, J.: A spectrometer for measuring particle size distributions in the range of 3 nm to 10 μm, *Front. Env. Sci. Eng.*, 10, 63–72, <https://doi.org/10.1007/s11783-014-0754-x>, 2016.
- Liu, Y., Yan, C., Feng, Z., Zheng, F., Fan, X., Zhang, Y., Li, C., Zhou, Y., Lin, Z., Guo, Y., Zhang, Y., Ma, L., Zhou, W., Liu, Z., Dada, L., Dällenbach, K., Kontkanen, J., Cai, R., Chan, T., Chu, B., Du, W., Yao, L., Wang, Y., Cai, J., Kangasluoma, J., Kokkonen, T., Kujansuu, J., Rusanen, A., Deng, C., Fu, Y., Yin, R., Li, X., Lu, Y., Liu, Y., Lian, C., Yang, D., Wang, W., Ge, M., Wang, Y., Worsnop, D. R., Junninen, H., He, H., Kerminen, V.-M., Zheng, J., Wang, L., Jiang, J., Petäjä, T., Bianchi, F., and Kulmala, M.: Continuous and comprehensive atmospheric observations in Beijing: a station to understand the complex urban atmospheric environment, *Big Earth Data*, 4, 295–321, <https://doi.org/10.1080/20964471.2020.1798707>, 2020.
- Liu, Y., Nie, W., Li, Y., Ge, D., Liu, C., Xu, Z., Chen, L., Wang, T., Wang, L., Sun, P., Qi, X., Wang, J., Xu, Z., Yuan, J., Yan, C., Zhang, Y., Huang, D., Wang, Z., Donahue, N. M., Worsnop, D., Chi, X., Ehn, M., and Ding, A.: Formation of condensable organic vapors from anthropogenic and biogenic volatile organic compounds (VOCs) is strongly perturbed by NO_x in eastern China, *Atmos. Chem. Phys.*, 21, 14789–14814, <https://doi.org/10.5194/acp-21-14789-2021>, 2021.
- Lu, Y., Yan, C., Fu, Y., Chen, Y., Liu, Y., Yang, G., Wang, Y., Bianchi, F., Chu, B., Zhou, Y., Yin, R., Baalbaki, R., Garmash, O., Deng, C., Wang, W., Liu, Y., Petäjä, T., Kerminen, V.-M., Jiang, J., Kulmala, M., and Wang, L.: A proxy for atmospheric daytime gaseous sulfuric acid concentration in urban Beijing, *Atmos. Chem. Phys.*, 19, 1971–1983, <https://doi.org/10.5194/acp-19-1971-2019>, 2019.
- Mahfouz, N. G. A. and Donahue, N. M.: Technical note: The enhancement limit of coagulation scavenging of small charged particles, *Atmos. Chem. Phys.*, 21, 3827–3832, <https://doi.org/10.5194/acp-21-3827-2021>, 2021.
- Mäkelä, J. M.: Biogenic iodine emissions and identification of end-products in coastal ultrafine particles during nucleation bursts, *J. Geophys. Res.*, 107, 8110, <https://doi.org/10.1029/2001jd000580>, 2002.
- Manninen, H. E., Mirme, S., Mirme, A., Petäjä, T., and Kulmala, M.: How to reliably detect molecular clusters and nucleation mode particles with Neutral cluster and Air Ion Spectrometer (NAIS), *Atmos. Meas. Tech.*, 9, 3577–3605, <https://doi.org/10.5194/amt-9-3577-2016>, 2016.
- McMurry, P. H., Fink, M., Sakurai, H., Stolzenburg, M. R., Mauldin, R. L., Smith, J., Eisele, F., Moore, K., Sjostedt, S., Tanner, D., Huey, L. G., Nowak, J. B., Edgerton, E., and Voisin, D.: A criterion for new particle formation in the sulfur-rich Atlanta atmosphere, *J. Geophys. Res.*, 110, D22S02, <https://doi.org/10.1029/2005jd005901>, 2005.
- Moore, R. M. and Zafiriou, O. C.: Photochemical Production of Methyl-Iodide in Seawater, *J. Geophys. Res.-Atmos.*, 99, 16415–16420, <https://doi.org/10.1029/94jd00786>, 1994.
- Nie, W., Yan, C., Huang, D. D., Wang, Z., Liu, Y., Qiao, X., Guo, Y., Tian, L., Zheng, P., Xu, Z., Li, Y., Xu, Z., Qi, X., Sun, P., Wang, J., Zheng, F., Li, X., Yin, R., Dällenbach, K. R., Bianchi, F., Petäjä, T., Zhang, Y., Wang, M., Schervish, M., Wang, S., Qiao, L., Wang, Q., Zhou, M., Wang, H., Yu, C., Yao, D., Guo, H., Ye, P., Lee, S., Li, Y. J., Liu, Y., Chi, X., Kerminen, V.-M., Ehn, M., Donahue, N. M., Wang, T., Huang, C., Kulmala, M., Worsnop, D., Jiang, J., and Ding, A.: Secondary organic aerosol formed by condensing anthropogenic vapours over China's megacities, *Nat. Geosci.*, 15, 255–261, <https://doi.org/10.1038/s41561-022-00922-5>, 2022.
- Nieminen, T., Lehtinen, K. E. J., and Kulmala, M.: Sub-10 nm particle growth by vapor condensation – effects of vapor molecule size and particle thermal speed, *Atmos. Chem. Phys.*, 10, 9773–9779, <https://doi.org/10.5194/acp-10-9773-2010>, 2010.

- Ning, A., Liu, L., Zhang, S., Yu, F., Du, L., Ge, M., and Zhang, X.: The critical role of dimethylamine in the rapid formation of iodic acid particles in marine areas, *npj Climate and Atmospheric Science*, 5, 92, <https://doi.org/10.1038/s41612-022-00316-9>, 2022.
- O'Dowd, C. D. and Hoffmann, T.: Coastal New Particle Formation: A Review of the Current State-Of-The-Art, *Environ. Chem.*, 2, 245–255, <https://doi.org/10.1071/en05077>, 2005.
- O'Dowd, C. D., Jimenez, J. L., Bahreini, R., Flagan, R. C., Seinfeld, J. H., Hämeri, K., Pirjola, L., Kulmala, M., Jennings, S. G., and Hoffmann, T.: Marine aerosol formation from biogenic iodine emissions, *Nature*, 417, 632–636, <https://doi.org/10.1038/nature00775>, 2002.
- Paasonen, P., Asmi, A., Petäjä, T., Kajos, M. K., Äijälä, M., Junninen, H., Holst, T., Abbatt, J. P. D., Arneth, A., Birmili, W., van der Gon, H. D., Hamed, A., Hoffer, A., Laakso, L., Laaksonen, A., Richard Leaitch, W., Plass-Dülmer, C., Pryor, S. C., Räisänen, P., Swietlicki, E., Wiedensohler, A., Worsnop, D. R., Kerminen, V.-M., and Kulmala, M.: Warming-induced increase in aerosol number concentration likely to moderate climate change, *Nat. Geosci.*, 6, 438–442, <https://doi.org/10.1038/ngeo1800>, 2013.
- Paasonen, P., Peltola, M., Kontkanen, J., Junninen, H., Kerminen, V.-M., and Kulmala, M.: Comprehensive analysis of particle growth rates from nucleation mode to cloud condensation nuclei in boreal forest, *Atmos. Chem. Phys.*, 18, 12085–12103, <https://doi.org/10.5194/acp-18-12085-2018>, 2018.
- Petäjä, T., Mauldin III, R. L., Kosciuch, E., McGrath, J., Nieminen, T., Paasonen, P., Boy, M., Adamov, A., Kotiaho, T., and Kulmala, M.: Sulfuric acid and OH concentrations in a boreal forest site, *Atmos. Chem. Phys.*, 9, 7435–7448, <https://doi.org/10.5194/acp-9-7435-2009>, 2009.
- Plane, J. M. C., Joseph, D. M., Allan, B. J., Ashworth, S. H., and Francisco, J. S.: An Experimental and Theoretical Study of the Reactions OIO + NO and OIO + OH, *J. Phys. Chem. A*, 110, 93–100, <https://doi.org/10.1021/jp055364y>, 2006.
- Qi, X. M., Ding, A. J., Nie, W., Petäjä, T., Kerminen, V.-M., Herrmann, E., Xie, Y. N., Zheng, L. F., Manninen, H., Aalto, P., Sun, J. N., Xu, Z. N., Chi, X. G., Huang, X., Boy, M., Virkkula, A., Yang, X.-Q., Fu, C. B., and Kulmala, M.: Aerosol size distribution and new particle formation in the western Yangtze River Delta of China: 2 years of measurements at the SORPES station, *Atmos. Chem. Phys.*, 15, 12445–12464, <https://doi.org/10.5194/acp-15-12445-2015>, 2015.
- Qiao, X., Yan, C., Li, X., Guo, Y., Yin, R., Deng, C., Li, C., Nie, W., Wang, M., Cai, R., Huang, D., Wang, Z., Yao, L., Worsnop, D. R., Bianchi, F., Liu, Y., Donahue, N. M., Kulmala, M., and Jiang, J.: Contribution of Atmospheric Oxygenated Organic Compounds to Particle Growth in an Urban Environment, *Environ. Sci. Technol.*, 55, 13646–13656, <https://doi.org/10.1021/acs.est.1c02095>, 2021.
- Redeker, K. R. and Cicerone, R. J.: Environmental controls over methyl halide emissions from rice paddies, *Global Biogeochem. Cy.*, 18, GB1027, <https://doi.org/10.1029/2003gb002092>, 2004.
- Redeker, K. R., Wang, N., Low, J. C., McMillan, A., Tyler, S. C., and Cicerone, R. J.: Emissions of methyl halides and methane from rice paddies, *Science*, 290, 966–969, <https://doi.org/10.1126/science.290.5493.966>, 2000.
- Saiz-Lopez, A., Plane, J. M., Baker, A. R., Carpenter, L. J., von Glasow, R., Martin, J. C., McFiggans, G., and Saunders, R. W.: Atmospheric chemistry of iodine, *Chem. Rev.*, 112, 1773–1804, <https://doi.org/10.1021/cr200029u>, 2012.
- Shi, X., Qiu, X., Chen, Q., Chen, S., Hu, M., Rudich, Y., and Zhu, T.: Organic Iodine Compounds in Fine Particulate Matter from a Continental Urban Region: Insights into Secondary Formation in the Atmosphere, *Environ. Sci. Technol.*, 55, 1508–1514, <https://doi.org/10.1021/acs.est.0c06703>, 2021.
- Sipilä, M., Sarnela, N., Jokinen, T., Henschel, H., Junninen, H., Kontkanen, J., Richters, S., Kangasluoma, J., Franchin, A., Peräkylä, O., Rissanen, M. P., Ehn, M., Vehkamäki, H., Kurten, T., Berndt, T., Petäjä, T., Worsnop, D., Ceburnis, D., Kerminen, V.-M., Kulmala, M., and O'Dowd, C.: Molecular-scale evidence of aerosol particle formation via sequential addition of HIO₃, *Nature*, 537, 532–534, <https://doi.org/10.1038/nature19314>, 2016.
- Sive, B. C., Varner, R. K., Mao, H., Blake, D. R., Wiggenter, O. W., and Talbot, R.: A large terrestrial source of methyl iodide, *Geophys. Res. Lett.*, 34, L17808, <https://doi.org/10.1029/2007gl030528>, 2007.
- Stolzenburg, D., Simon, M., Ranjithkumar, A., Kürten, A., Lehtipalo, K., Gordon, H., Ehrhart, S., Finkenzeller, H., Pichelstorfer, L., Nieminen, T., He, X.-C., Brilke, S., Xiao, M., Amorim, A., Baalbaki, R., Baccarini, A., Beck, L., Bräkling, S., Caudillo Murillo, L., Chen, D., Chu, B., Dada, L., Dias, A., Dommen, J., Duplissy, J., El Haddad, I., Fischer, L., Gonzalez Carracedo, L., Heinritzi, M., Kim, C., Koenig, T. K., Kong, W., Lamkaddam, H., Lee, C. P., Leiminger, M., Li, Z., Makhmutov, V., Manninen, H. E., Marie, G., Marten, R., Müller, T., Nie, W., Partoll, E., Petäjä, T., Pfeifer, J., Philippov, M., Rissanen, M. P., Rörup, B., Schobesberger, S., Schuchmann, S., Shen, J., Sipilä, M., Steiner, G., Stozhkov, Y., Tauber, C., Tham, Y. J., Tomé, A., Vazquez-Pufleau, M., Wagner, A. C., Wang, M., Wang, Y., Weber, S. K., Wimmer, D., Wlasits, P. J., Wu, Y., Ye, Q., Zauner-Wieczorek, M., Baltensperger, U., Carslaw, K. S., Curtius, J., Donahue, N. M., Flagan, R. C., Hansel, A., Kulmala, M., Lelieveld, J., Volkamer, R., Kirkby, J., and Winkler, P. M.: Enhanced growth rate of atmospheric particles from sulfuric acid, *Atmos. Chem. Phys.*, 20, 7359–7372, <https://doi.org/10.5194/acp-20-7359-2020>, 2020.
- Thakur, R. C., Dada, L., Beck, L. J., Quéléver, L. L. J., Chan, T., Marbouti, M., He, X.-C., Xavier, C., Sulo, J., Lampilahti, J., Lampimäki, M., Tham, Y. J., Sarnela, N., Lehtipalo, K., Norkko, A., Kulmala, M., Sipilä, M., and Jokinen, T.: An evaluation of new particle formation events in Helsinki during a Baltic Sea cyanobacterial summer bloom, *Atmos. Chem. Phys.*, 22, 6365–6391, <https://doi.org/10.5194/acp-22-6365-2022>, 2022.
- Tomasi, C. and Lupi, A.: Primary and Secondary Sources of Atmospheric Aerosol, in: *Atmospheric Aerosols*, Wiley-VCH, 1–86, <https://doi.org/10.1002/9783527336449.ch1>, 2017.
- Tröstl, J., Chuang, W. K., Gordon, H., Heinritzi, M., Yan, C., Molteni, U., Ahlm, L., Frege, C., Bianchi, F., Wagner, R., Simon, M., Lehtipalo, K., Williamson, C., Craven, J. S., Duplissy, J., Adamov, A., Almeida, J., Bernhammer, A.-K., Breitenlechner, M., Brilke, S., Dias, A., Ehrhart, S., Flagan, R. C., Franchin, A., Fuchs, C., Guida, R., Gysel, M., Hansel, A., Hoyle, C. R., Jokinen, T., Junninen, H., Kangasluoma, J., Keskinen, H., Kim, J., Krapf, M., Kürten, A., Laaksonen, A., Lawler, M., Leiminger, M., Mathot, S., Möhler, O., Nieminen, T., Onnela, A., Petäjä, T., Piel, F. M., Miettinen, P., Rissanen, M. P.,

- Rondo, L., Sarnela, N., Schobesberger, S., Sengupta, K., Sipilä, M., Smith, J. N., Steiner, G., Tomè, A., Virtanen, A., Wagner, A. C., Weingartner, E., Wimmer, D., Winkler, P. M., Ye, P., Carslaw, K. S., Curtius, J., Dommen, J., Kirkby, J., Kulmala, M., Riipinen, I., Worsnop, D. R., Donahue, N. M., and Baltensperger, U.: The role of low-volatility organic compounds in initial particle growth in the atmosphere, *Nature*, 533, 527–531, <https://doi.org/10.1038/nature18271>, 2016.
- Veli-Matti Kerminen, M. K.: Analytical formulae connecting the “real” and the “apparent” nucleation rate and the nuclei number concentration for atmospheric nucleation events, *J. Aerosol Sci.*, 33, 609–622, 2002.
- Wang, Q., Yan, D., Wang, X., Lu, P., Li, X., and Cao, A.: Research advances in soil fumigants, *Acta Phytophylacica Sinica*, 44, 529–543, 2017.
- Wang, Z., Zheng, F., Zhang, W., and Wang, S.: Analysis of SO₂ Pollution Changes of Beijing-Tianjin-Hebei Region over China Based on OMI Observations from 2006 to 2017, *Adv. Meteorol.*, 2018, 1–15, <https://doi.org/10.1155/2018/8746068>, 2018.
- Wehner, B., Siebert, H., Stratmann, F., Tuch, T., Wiedensohler, A., Petäjä, T., Dal Maso, M., and Kulmala, M.: Horizontal homogeneity and vertical extent of new particle formation events, *Tellus B*, 59, 362–371, <https://doi.org/10.1111/j.1600-0889.2007.00260.x>, 2007.
- Williams, J., Gros, V., Atlas, E., Maciejczyk, K., Batsaikhan, A., Schöler, H. F., Forster, C., Quack, B., Yassaa, N., Sander, R., and Van Dingenen, R.: Possible evidence for a connection between methyl iodide emissions and Saharan dust, *J. Geophys. Res.*, 112, D07302, <https://doi.org/10.1029/2005jd006702>, 2007.
- Wu, Z., Hu, M., Liu, S., Wehner, B., Bauer, S., Maßling, A., Wiedensohler, A., Petäjä, T., Dal Maso, M., and Kulmala, M.: New particle formation in Beijing, China: Statistical analysis of a 1-year data set, *J. Geophys. Res.*, 112, D09209, <https://doi.org/10.1029/2006jd007406>, 2007.
- Xiao, M., Hoyle, C. R., Dada, L., Stolzenburg, D., Kürten, A., Wang, M., Lamkaddam, H., Garmash, O., Mentler, B., Molteni, U., Baccarini, A., Simon, M., He, X.-C., Lehtipalo, K., Ahonen, L. R., Baalbaki, R., Bauer, P. S., Beck, L., Bell, D., Bianchi, F., Brilke, S., Chen, D., Chiu, R., Dias, A., Duplissy, J., Finkenzeller, H., Gordon, H., Hofbauer, V., Kim, C., Koenig, T. K., Lampilahti, J., Lee, C. P., Li, Z., Mai, H., Makhmutov, V., Manninen, H. E., Marten, R., Mathot, S., Mauldin, R. L., Nie, W., Onnela, A., Partoll, E., Petäjä, T., Pfeifer, J., Pospisilova, V., Quéléver, L. L. J., Rissanen, M., Schobesberger, S., Schuchmann, S., Stozhkov, Y., Tauber, C., Tham, Y. J., Tomé, A., Vazquez-Pufleau, M., Wagner, A. C., Wagner, R., Wang, Y., Weitz, L., Wimmer, D., Wu, Y., Yan, C., Ye, P., Ye, Q., Zha, Q., Zhou, X., Amorim, A., Carslaw, K., Curtius, J., Hansel, A., Volkamer, R., Winkler, P. M., Flagan, R. C., Kulmala, M., Worsnop, D. R., Kirkby, J., Donahue, N. M., Baltensperger, U., El Haddad, I., and Dommen, J.: The driving factors of new particle formation and growth in the polluted boundary layer, *Atmos. Chem. Phys.*, 21, 14275–14291, <https://doi.org/10.5194/acp-21-14275-2021>, 2021.
- Yan, C., Yin, R., Lu, Y., Dada, L., Yang, D., Fu, Y., Kontkanen, J., Deng, C., Garmash, O., Ruan, J., Baalbaki, R., Schervish, M., Cai, R., Bloss, M., Chan, T., Chen, T., Chen, Q., Chen, X., Chen, Y., Chu, B., Dällenbach, K., Foreback, B., He, X., Heikkinen, L., Jokinen, T., Junninen, H., Kangasluoma, J., Kokkonen, T., Kurppa, M., Lehtipalo, K., Li, H., Li, H., Li, X., Liu, Y., Ma, Q., Paasonen, P., Rantala, P., Pileci, R. E., Rusanen, A., Sarnela, N., Simonen, P., Wang, S., Wang, W., Wang, Y., Xue, M., Yang, G., Yao, L., Zhou, Y., Kujansuu, J., Petäjä, T., Nie, W., Ma, Y., Ge, M., He, H., Donahue, N. M., Worsnop, D. R., Veli-Matti, K., Wang, L., Liu, Y., Zheng, J., Kulmala, M., Jiang, J., and Bianchi, F.: The Synergistic Role of Sulfuric Acid, Bases, and Oxidized Organics Governing New-Particle Formation in Beijing, *Geophys. Res. Lett.*, 48, e2020GL091944, <https://doi.org/10.1029/2020gl091944>, 2021.
- Yang, L., Nie, W., Liu, Y., Xu, Z., Xiao, M., Qi, X., Li, Y., Wang, R., Zou, J., Paasonen, P., Yan, C., Xu, Z., Wang, J., Zhou, C., Yuan, J., Sun, J., Chi, X., Kerminen, V. M., Kulmala, M., and Ding, A.: Toward Building a Physical Proxy for Gas-Phase Sulfuric Acid Concentration Based on Its Budget Analysis in Polluted Yangtze River Delta, East China, *Environ. Sci. Technol.*, 55, 6665–6676, <https://doi.org/10.1021/acs.est.1c00738>, 2021.
- Yang, X., Xiao, D., Bai, H., Tang, J., and Wang, W.: Spatiotemporal Distributions of PM_{2.5} Concentrations in the Beijing–Tianjin–Hebei Region From 2013 to 2020, *Front. Environ. Sci.*, 10, 843862, <https://doi.org/10.3389/fenvs.2022.842237>, 2022.
- Yao, L., Garmash, O., Bianchi, F., Zheng, J., Yan, C., Kontkanen, J., Junninen, H., Mazon, S. B., Ehn, M., Paasonen, P., Sipilä, M., Wang, M., Wang, X., Xiao, S., Chen, H., Lu, Y., Zhang, B., Wang, D., Fu, Q., Geng, F., Li, L., Wang, H., Qiao, L., Yang, X., Chen, J., Kerminen, V.-M., Petäjä, T., Worsnop, D. R., Kulmala, M., and Wang, L.: Atmospheric new particle formation from sulfuric acid and amines in a Chinese megacity, *Science*, 361, 278–281, <https://doi.org/10.1126/science.aao4839>, 2018.
- Yokouchi, Y., Osada, K., Wada, M., Hasebe, F., Agama, M., Murakami, R., Mukai, H., Nojiri, Y., Inuzuka, Y., Toom-Saunty, D., and Fraser, P.: Global distribution and seasonal concentration change of methyl iodide in the atmosphere, *J. Geophys. Res.*, 113, D18311, <https://doi.org/10.1029/2008jd009861>, 2008.
- Yokouchi, Y., Nojiri, Y., Toom-Saunty, D., Fraser, P., Inuzuka, Y., Tanimoto, H., Nara, H., Murakami, R., and Mukai, H.: Long-term variation of atmospheric methyl iodide and its link to global environmental change, *Geophys. Res. Lett.*, 39, L23805, <https://doi.org/10.1029/2012gl053695>, 2012.
- Zhang, R., Xie, H. B., Ma, F., Chen, J., Iyer, S., Simon, M., Heinritzi, M., Shen, J., Tham, Y. J., Kurtén, T., Worsnop, D. R., Kirkby, J., Curtius, J., Sipilä, M., Kulmala, M., and He, X. C.: Critical Role of Iodous Acid in Neutral Iodine Oxoacid Nucleation, *Environ. Sci. Technol.*, 56, 14166–14177, <https://doi.org/10.1021/acs.est.2c04328>, 2022.
- Zhou, Y., Hakala, S., Yan, C., Gao, Y., Yao, X., Chu, B., Chan, T., Kangasluoma, J., Gani, S., Kontkanen, J., Paasonen, P., Liu, Y., Petäjä, T., Kulmala, M., and Dada, L.: Measurement report: New particle formation characteristics at an urban and a mountain station in northern China, *Atmos. Chem. Phys.*, 21, 17885–17906, <https://doi.org/10.5194/acp-21-17885-2021>, 2021.